Published March 23, 2015

Rab8, POSH, and TAK1 regulate synaptic growth in a *Drosophila* model of frontotemporal dementia

Ryan J.H. West,[1,2] Yubing Lu,[3] Bruno Marie,[4] Fen-Biao Gao,[3] and Sean T. Sweeney[1,2]

[1]Department of Biology and [2]Hull York Medical School, University of York, Heslington, York YO10 5DD, England, UK
[3]Department of Neurology, University of Massachusetts Medical School, Worcester, MA 01605
[4]Institute of Neurobiology, Medical Sciences Campus, University of Puerto Rico, San Juan, Puerto Rico 00901

Mutations in genes essential for protein homeostasis have been identified in frontotemporal dementia (FTD) and amyotrophic lateral sclerosis (ALS) patients. Why mature neurons should be particularly sensitive to such perturbations is unclear. We identified mutations in *Rab8* in a genetic screen for enhancement of an FTD phenotype associated with ESCRT-III dysfunction. Examination of *Rab8* mutants or motor neurons expressing a mutant ESCRT-III subunit, CHMP2B^{Intron5}, at the *Drosophila melanogaster* neuromuscular junction synapse revealed synaptic overgrowth and endosomal dysfunction. Expression of Rab8 rescued overgrowth phenotypes generated by CHMP2B^{Intron5}. In *Rab8* mutant synapses, c-Jun N-terminal kinase (JNK)/activator protein-1 and TGF-β signaling were overactivated and acted synergistically to potentiate synaptic growth. We identify novel roles for endosomal JNK-scaffold POSH (Plenty-of-SH3s) and a JNK kinase kinase, TAK1, in regulating growth activation in *Rab8* mutants. Our data uncover Rab8, POSH, and TAK1 as regulators of synaptic growth responses and point to recycling endosome as a key compartment for synaptic growth regulation during neurodegenerative processes.

Introduction

Frontotemporal dementia (FTD) is the second most prevalent form of early onset dementia after Alzheimer's disease, accounting for up to 20% of all dementia cases under 65 yr of age (Van Langenhove et al., 2012). FTD is highly heterogeneous, presenting broad clinical, pathological, and genetic disparity among affected individuals (Hardy and Rogaeva, 2013; Ling et al., 2013). Molecular and genetic studies have identified several loci implicated in the disease, the most common being *MAPT* (Hutton et al., 1998), *GRN* (Baker et al., 2006; Cruts et al., 2006), and *C9ORF72* (DeJesus-Hernandez et al., 2011; Renton et al., 2011). Less common loci include *TARDBP* (Borroni et al., 2009; Kovacs et al., 2009), *VCP* (Watts et al., 2004), and *CHMP2B* (Skibinski et al., 2005). A growing body of evidence supports the idea that FTD is clinically, pathologically and mechanistically linked with amyotrophic lateral sclerosis (ALS; Ringholz and Greene, 2006; Wheaton et al., 2007; Hardy and Rogaeva, 2013; Ling et al., 2013) in which FTD and ALS constitute extremes of a continuum, representing a single neurodegenerative disorder (Ling et al., 2013).

CHMP2B encodes a component of the ESCRT-III complex that acts sequentially with ESCRT-0, -I, and -II and is essential for the biogenesis of multivesicular bodies (MVBs; Henne et al., 2011). Mutations in *CHMP2B* have been identified in FTD and ALS patients (Skibinski et al., 2005; Parkinson et al., 2006; Cox et al., 2010; van Blitterswijk et al., 2012). MVBs provide a sorting nexus for both endosomal–lysosomal and autophagic trafficking pathways, critical for protein homeostasis and regulation of signaling. In support of this, CHMP2B function has been implicated in autophagosome maturation (Filimonenko et al., 2007; Lee et al., 2007; Rusten et al., 2007; Lu et al., 2013). The dominant pathological *CHMP2B^{Intron5}* mutation generates a C-terminally truncated CHMP2B protein, which forms a more avid association with ESCRT-III component Snf-7/CHMP4B, inhibiting dissociation of the ESCRT-III complex (Lee et al., 2007). The *CHMP2B^{Intron5}* mutation therefore perturbs normal endosomal trafficking, resulting in autophagosome accumulation and neurodegeneration (Lee et al., 2007; Urwin et al., 2010).

Correspondence to Sean T. Sweeney: sean.sweeney@york.ac.uk

Abbreviations used in this paper: ALS, amyotrophic lateral sclerosis; AP-1, activator protein-1; EPSP, excitatory postsynaptic potential; Eve, even-skipped; FTD, frontotemporal dementia; GMR, glass multimer reporter; Hiw, highwire; JNKKK, JNK kinase kinase; LAMP, lysosome-associated membrane protein; MCC, Mander's correlation coefficient; mEPSP, miniature EPSP; MVB, multivesicular body; NMJ, neuromuscular junction; PCC, Pearson's correlation coefficient; P-MAD, phosphorylated MAD; UAS, upstream activation sequence; VNC, ventral nerve cord; Wit, wishful thinking.

The Rockefeller University Press $30.00
J. Cell Biol.
www.jcb.org/cgi/doi/10.1083/jcb.201404066

Published March 23, 2015

Why neuronal subtypes in adults are particularly sensitive to perturbations in ESCRT-III function is not clear.

To address this question, we have previously established a *Drosophila melanogaster* model of FTD in which *CHMP2B*^{Intron5} is expressed in postmitotic neurons in the eye (Ahmad et al., 2009). A genetic screen has so far identified *Serpin5*, a negative regulator of the Toll receptor activated innate immune pathway and *Syntaxin13*, required for autophagosome maturation, as dominant enhancers of *CHMP2B*^{Intron5} toxicity (Ahmad et al., 2009; Lu et al., 2013). Here, we describe the identification and characterization of mutations in the small endosomal GTPase *Rab8* as another distinct modifier of the *CHMP2B*^{Intron5} phenotype.

In vitro studies have previously shown Rab8 playing an important role in exocytic membrane traffic from the Golgi complex in polarized epithelial cells (Huber et al., 1993b), photoreceptor cells (Moritz et al., 2001), and neurons (Huber et al., 1993a). Similar in vitro studies have demonstrated a regulatory role for Rab8 in the cycling and delivery of α-amino-3-hydroxy-5-methyl-4-isoxazolepropionic acid and metabotropic glutamate receptors into dendritic spines in an endosome-dependent manner (Brown et al., 2007; Esseltine et al., 2012). In vertebrates, genetic analysis of neuronal Rab8 function has been hampered by the presence of two Rab8 isoforms, Rab8a and Rab8b, that may compensate for each other (Sato et al., 2014). In addition, *Rab8* knockout mice typically die prematurely, as a result of nutritional wasting associated with the role of Rab8 in the development of intestinal epithelial cells (Sato et al., 2007), preventing study of Rab8 function in neurons.

Here, we demonstrate that heterozygous *Rab8* mutants dominantly enhance *CHMP2B*^{Intron5} toxicity in our *Drosophila* model of FTD. We identify mutations in the single *Drosophila Rab8* gene and show that *Rab8* mutants display significant perturbations to normal endosomal trafficking within motor neurons, leading to misregulated TGF-β and JNK signaling. This misregulation results in aberrant synaptic overgrowth at the *Drosophila* neuromuscular junction (NMJ) synapse, a hallmark of neurodegenerative disease in *Drosophila* models. Synaptic overgrowth in *Rab8* mutants can be alleviated through reduction of POSH (Plenty of SH3's), an endosomal JNK scaffold (Tapon et al., 1998; Xu et al., 2003; Tsuda et al., 2006; Votteler et al., 2009) that aggregates within axon bundles of *Rab8* mutants. Expression of CHMP2B^{intron5} in motor neurons also increases synaptic growth and TGF-β and JNK signaling, phenotypes that are reversed by the coexpression of Rab8. We present POSH as a novel nexus linking activity of TGF-β and JNK signaling via TAK1 (TGF-β–activated kinase 1), a JNK kinase kinase (JNKKK) essential for synaptic overgrowth in *Rab8* mutants. Thus, we provide evidence for a novel pathway regulating synaptic growth in both normal development and in a synaptic overgrowth disease model.

Results

A genetic screen in *Drosophila* identifies *Rab8* as a dominant enhancer of mutant *CHMP2B* toxicity

Expression of *CHMP2B*^{Intron5} in the *Drosophila* eye, under the control of the postmitotic eye-specific driver glass multimer reporter (*GMR*)-Gal4, leads to a mild phenotype characterized by melanotic deposits (Fig. 1 B; Ahmad et al., 2009; Lu et al., 2013). Loss of one copy of the deficiency allele *Df(3L)ED228* (Fig. 1, A–C) potentiated this phenotype. To identify the genes responsible for this genetic interaction, mutant alleles of individual genes within this deficiency region were screened against the *CHMP2B*^{Intron5} eye phenotype. The *Rab8*^{1} allele significantly potentiated *CHMP2B*^{Intron5} toxicity (Fig. 1, B and C). Enhancement was consistent for four additional identified *Rab8* mutant alleles (Figs. 1 D and S1) as well as *Rab8*-RNAi expression (Fig. 1, B and C). In addition, coexpression of wild-type *Rab8* with *CHMP2B*^{Intron5} could partially alleviate toxicity (Fig. S1 C). Sequencing of identified *Rab8* alleles revealed missense mutations (Figs. 1 D and S1) affecting conserved residues essential for Rab8 GTPase function (Fig. S1; Giagtzoglou et al., 2012). Complementation analysis demonstrated that all *Rab8* mutant combinations die at the pharate pupal stage (Figs. 1 E and S1 B).

Presynaptic *Rab8* regulates NMJ synapse development

Rab8 function in *Drosophila*, and in neurons in general, is poorly understood. We first examined whether *Rab8* is expressed in motor neurons. Expression of the membrane-associated GFP, mCD8-GFP, under the control of the *Rab8*-GAL4 driver (Chan et al., 2011) revealed *Rab8* expressed throughout the *Drosophila* larval ventral nerve cord (VNC), with coexpression in all even-skipped (Eve)–positive cells (Fig. 2 A), indicating expression in all motor neurons.

To examine potential roles for *Rab8* in synaptic growth and function, we used the *Drosophila* third instar larval NMJ as a model synapse. All trans-heterozygous allelic combinations of *Rab8* mutants presented with synaptic overgrowth, characterized by significant increase in synaptic bouton number of up to 100% (Fig. 2, B and C). With the *Rab8*^{1} allele previously identified as a hypomorph (Giagtzoglou et al., 2012), the observation of synaptic overgrowth in all trans-heterozygote combinations of *Rab8* alleles strongly associates synaptic overgrowth with loss of *Rab8* function. Synaptic overgrowth observed was highly penetrant affecting every NMJ observed, including both muscles 6/7 and 4 (Fig. 2, B–E).

We hereafter chose to focus on *Rab8*^{1}/*Rab8*^{B229} trans-heterozygotes as a robust representative of *Rab8* synapse overgrowth. To determine whether Rab8 has a pre- or postsynaptic role in the regulation of synaptic growth, genetic rescue experiments were performed. Both global (*actin*-Gal4) and presynaptic (*neuronal-synaptobrevin/n-Syb*–Gal4) expression of upstream activation sequence (UAS)–*Rab8* were sufficient to completely rescue increased synaptic bouton number at both muscles 6/7 and 4 (Fig. 2, D and E). In contrast, postsynaptic (*MHC*-Gal4) expression of UAS-*Rab8* rescued increased synaptic bouton number, but not synapse length at muscle 6/7 (Fig. 2, C and D; and Fig. S2). Synaptic bouton number or length, in muscle 4 was not rescued by muscle expression of Rab8 (Fig. 2, C and E; and Fig. S2). In addition to elevated bouton number, *Rab8* mutants also have a significant increase in NMJ length, branching, and satellite bouton number, with a reduction in synaptic bouton size (Fig. S2). These phenotypes were completely rescued by both global and presynaptic, but not postsynaptic, expression of *Rab8*. Collectively, these results indicate a presynaptic role for Rab8 in the regulation of synaptic growth.

Published March 23, 2015

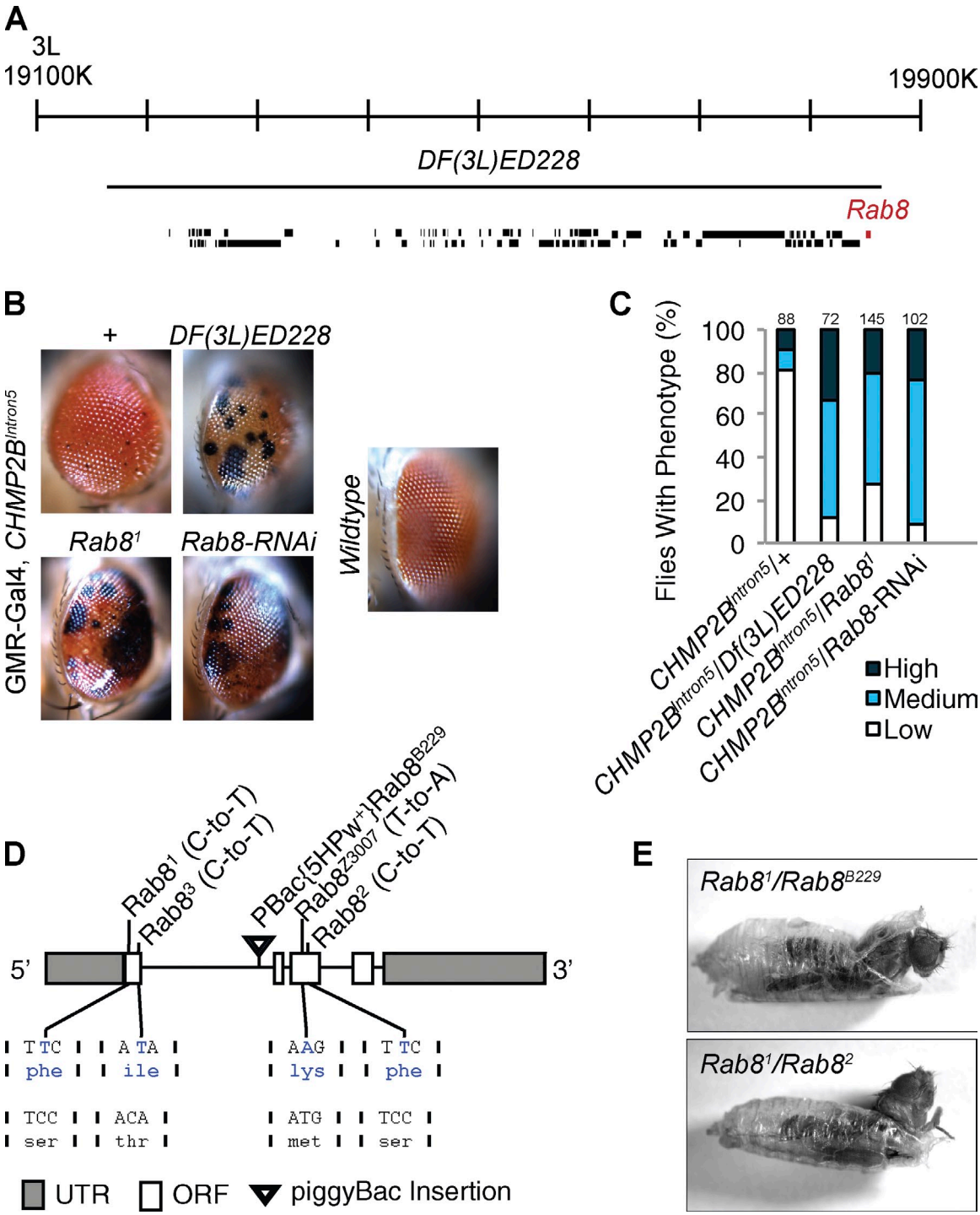

Figure 1. **A genetic screen identifies *Rab8* mutants as dominant enhancers of *CHMP2B*^{Intron5} toxicity.** (A) Schematic representation of the genomic region uncovered by the *Df(3L)ED228* deficiency. (B) *Df(3L)ED228*, *Rab8*^{1}/+, or *Rab8*-RNAi expression dominantly enhance the *CHMP2B*^{Intron5} mutant eye phenotype, with increased melanization. (C) Quantification of the eye phenotype in flies for genotypes in B. Numbers above bars = *n*. (D) Schematic representation of the *Rab8* locus with location and nature of *Rab8* mutant alleles used in this study. (E) *Rab8* trans-heterozygote mutant combinations show pharate lethality.

Rab8 is localized to the synaptic recycling endosome

Although it has previously been reported that Rab8 has a role in neurite outgrowth (Huber et al., 1993a) and neurotransmitter receptor recycling in neurons (Gerges et al., 2004; Esseltine et al., 2012) via a function in the recycling endosome (Brown et al., 2007), it is not clear how these effects are mediated. We find that expressed YFP-tagged Rab8 partially colocalizes with markers for the slow (Rab11) and fast (Rab4) recycling endosome in motor neurons, in addition to the synaptic TGF-β type II receptor, wishful thinking (Wit; Fig. 3, A–C; Aberle et al., 2002; Marqués et al., 2002), indicating function in the recycling endosome at the synapse, a compartment previously associated with synaptic growth control via regulation of TGF-β receptor traffic (Rodal et al., 2011).

Published March 23, 2015

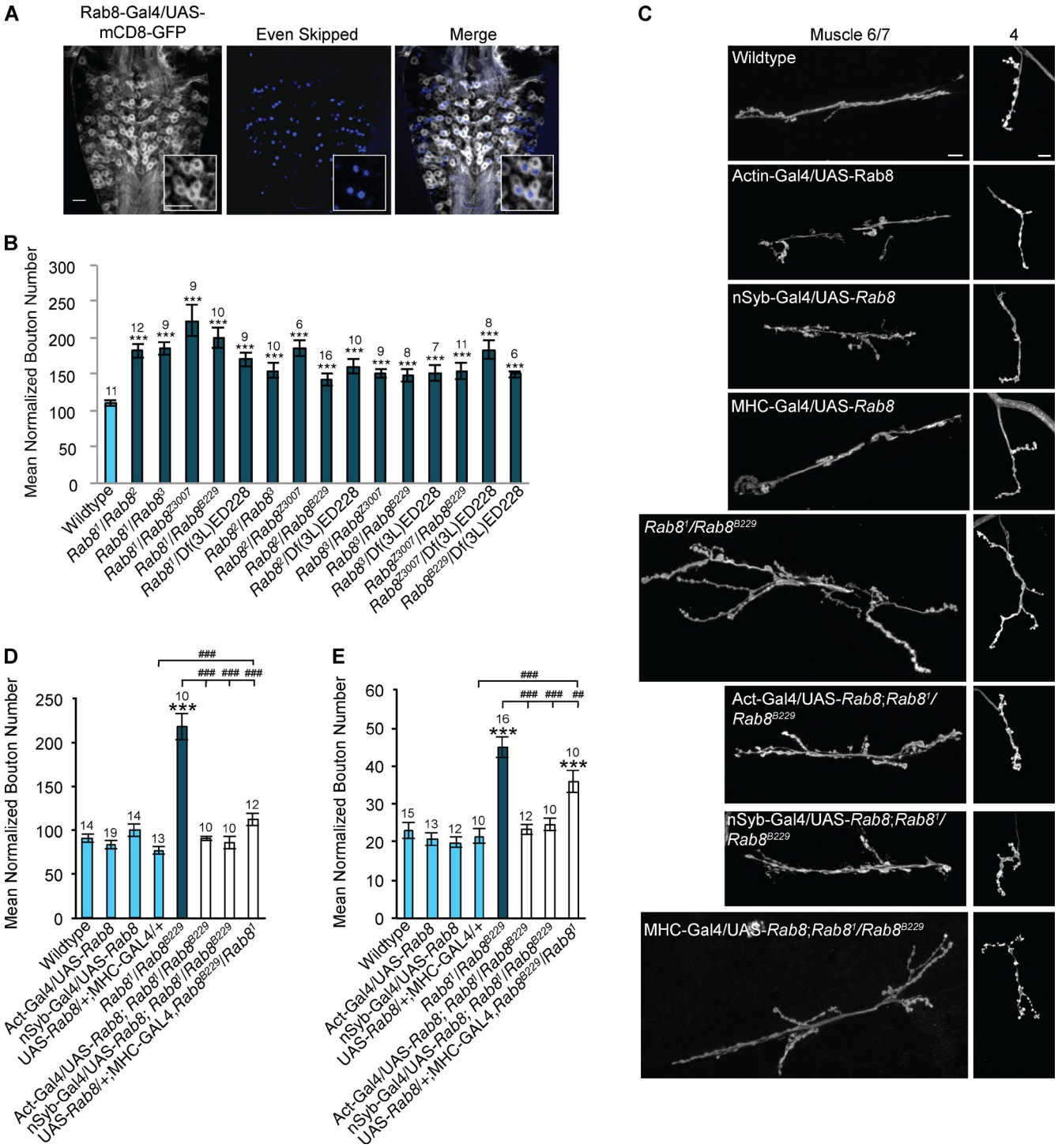

Figure 2. ***Rab8* mutants reveal a presynaptic role for Rab8 in the regulation of neuronal growth at the larval NMJ.** (A) Rab8 is expressed in all Eve-positive motor neurons within the third instar larval VNC. Insets show magnification of four neurons showing coexpression of eve and Rab8 promoter–driven mCD8-GFP. Bar, 20 µm. (B) All trans-heterozygous *Rab8* mutant combinations show significant synaptic overgrowth at the third instar larval NMJ (muscle 6/7, hemisegment A3). ANOVA: F(d.f. [degrees of freedom] 15) = 10.14; ***, P < 0.001 with post-hoc Dunnett's comparison to wild-type control. (C) Overgrowth can be completely rescued by global (*actin*-Gal4) and neuronal (*n-Syb*–Gal4) expression of UAS-*Rab8*. Muscle (*MHC*-Gal4) expression of UAS-*Rab8* partially rescues synaptic bouton number in Rab8 mutants. Bars, 10 µm. (D) Quantification of synaptic bouton number at muscle 6/7, hemisegment A3. ANOVA: F(d.f. 7) = 36.8975; ***, P < 0.001 with post-hoc Dunnett's comparison to wild-type control, and post-hoc Student's *t* test comparison between groups; ###, P < 0.001. (E) Quantification of synaptic bouton number at muscle 4, hemisegment A3. (ANOVA: F(d.f. 7) = 19.95; ***, P < 0.001 with post-hoc Dunnett's comparison to wild-type control, and post-hoc Student's *t* test comparison between groups; ###, P < 0.001; ##, P < 0.01. Numbers above bars = *n*. Error bars show SEM.

Published March 23, 2015

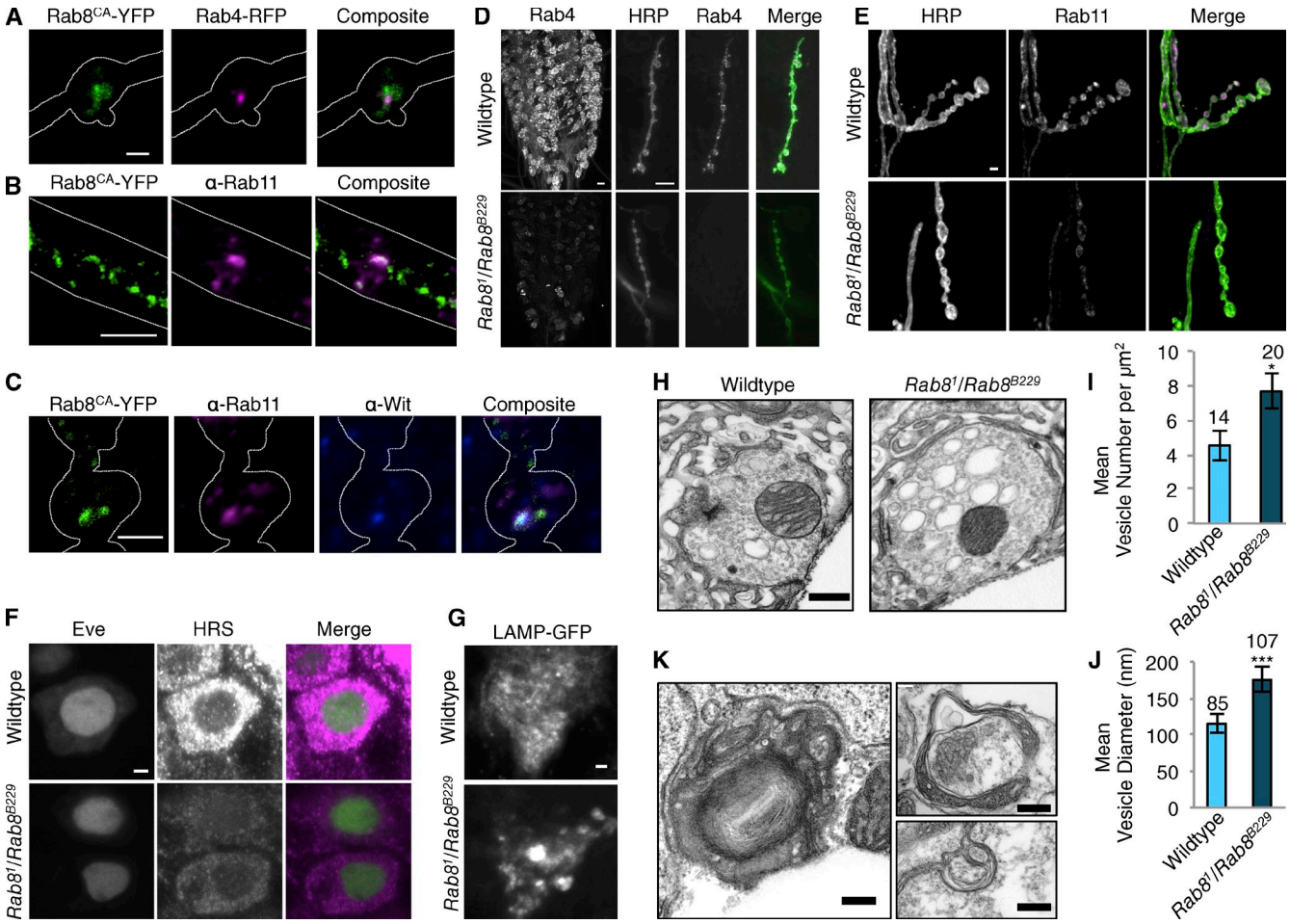

Figure 3. **Rab8 localizes to the recycling endosome at synapses and disruption of Rab8 function perturbs normal endosomal structure throughout the nervous system.** (A) Panneuronal (*n-Syb*–Gal4) expression of constitutively active Rab8-YFP ($Rab8^{CA}$-YFP) reveals colocalization of Rab8 with recycling endosomal marker Rab4-RFP, at the NMJ. White line defines outline of synaptic bouton. PCC: 0.59 ± 0.023 (mean ± SEM); Mander's correlation coefficient (MCC) M1: 0.73 ± 0.025; M2: 0.84 ± 0.034; *n* = 20. (B) $Rab8^{CA}$-YFP expressed with *n-syb*–GAL4 colocalizes with recycling endosome marker Rab11-GFP in the axon. White lines define outline of axon. (C) $Rab8^{CA}$-YFP expressed with *n-syb*–GAL4 colocalizes with Rab11-GFP (PCC: 0.65 ± 0.01; MCC M1: 0.87 ± 0.038; M2: 0.84 ± 0.034; *n* = 20) and TGF-β receptor Wit at the NMJ. White line defines the outline of synaptic bouton. (D) *Rab8* mutants show a reduction in the fast recycling endosome marker Rab4-RFP (expressed with *n-Syb*–GAL4) throughout the larval VNC and at the NMJ. (E) *Rab8* mutants show a reduction in the slow recycling endosome marker Rab11-EGFP (expressed with *n-Syb*–GAL4) at the NMJ. (F) *Rab8* mutants show decreased levels of HRS within the cell bodies of Eve-positive motor neurons of third instar larvae. (G) The late endosome marker LAMP accumulates in puncta within the VNC when expressed with *n-syb*–GAL4 in *Rab8* mutants. (H–J) Ultrastructural analysis of the larval NMJ synapse in *Rab8* mutants reveals a significant increase in large clear endosome-like structures (>70 nm) within synaptic boutons. Third instar larvae, muscle 6/7, hemisegment A3. (I) ANOVA: F(d.f.1) = 4.9635; *, P < 0.05. (J) ANOVA: F(d.f.1) = 55.1122; ***, P < 0.001. (K) Ultrastructural analysis in the VNC in third instar larvae of *Rab8* mutants uncovers large, aberrant, multilamellar, membranous structures not observed in wild-type animals. Numbers above bars = *n*. Error bars show SEM. Bars: (A and C–G) 2 µm; (B) 5 µm; (H) 500 nm; (K) 200 nm.

Rab8 mutants show endosomal perturbations

To understand how loss of Rab8 in neurons leads to synaptic overgrowth, we analyzed synapses at the endosomal and ultrastructural level. *Rab8* mutants displayed a clear reduction in both Rab11 and Rab4 recycling endosome markers at both the NMJ and in motor neuron cell bodies in the VNC (Fig. 3, D and E; and Fig. S3, A and B). In addition to depletion of recycling endosome markers, we found the ESCRT-0 subunit HRS, which is essential for MVB biogenesis, was also depleted within the cell body of Eve-positive motor neurons in *Rab8* mutants (Figs. 3 F and S3 C).

Upon ultrastructural analysis of the *Rab8* mutant synapse, accumulation of large endosome-like, intermediary structures within synaptic boutons was observed (Fig. 3, H–J), morphologically similar to those previously seen with manipulations of endocytic machinery such as Rab5 (Shimizu et al., 2003), clathrin (Kasprowicz et al., 2008; Kawasaki et al., 2011), AP180 (Zhang et al., 1998), and Dap160 (Winther et al., 2013). The structures we observe are, however, dissimilar and unlikely to be synaptic vesicles as they are not released; we did not observe any increase in quantal size during our electrophysiological analysis. On the contrary, *Rab8* mutants show decreased quantal size (Fig. 4). Multilamellar accumulations, consistent in size and distribution with lysosome-associated membrane protein (LAMP)–GFP accumulation (Fig. 3, G and K) were also observed within cell bodies of the larval VNC of *Rab8* mutant larvae. These structures are similar to the autophagosomal

Published March 23, 2015

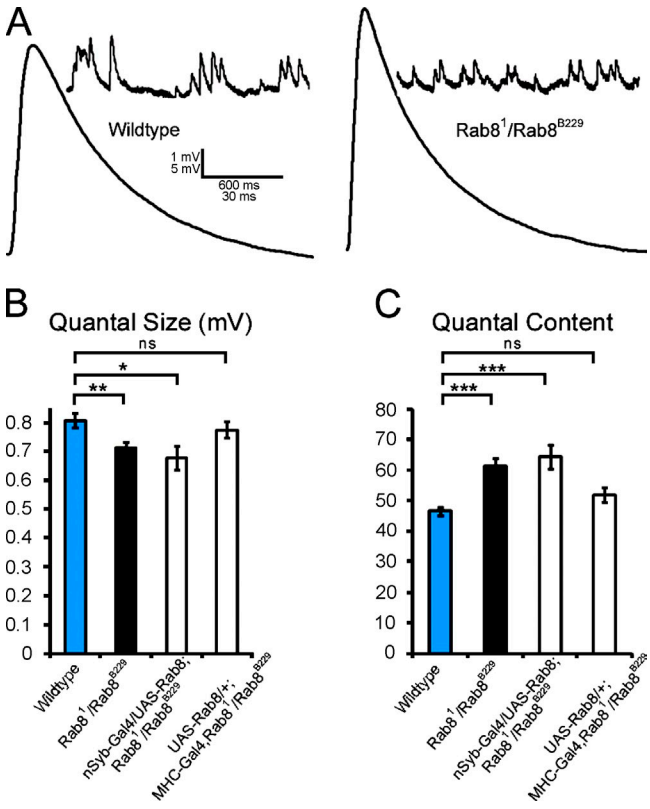

Figure 4. ***Rab8* mutants show decreased amplitude of spontaneous miniature release events and an increase in quantal content.** (A) Representative traces of miniature spontaneous release events and evoked EPSP in wild type and *Rab8* mutants. (B) Quantification of mean mEPSP amplitude in control and *Rab8* mutants. The mean amplitude of spontaneous miniature release events of *Rab8* mutants (0.71 ± 0.02 mV; $n = 21$) is decreased (Student's *t* test; $P < 0.006$) when compared with controls (0.81 ± 0.02 mV; $n = 22$). This decrease is not rescued by Rab8 expression in the neuron (mEPSP is 0.68 ± 0.04 mV; $n = 12$) but is rescued by expression of *Rab8* in muscle (mEPSP is 0.78 ± 0.03 mV; $n = 11$), showing that postsynaptic function of Rab8 is responsible for decreased miniature amplitude. (C) Quantification of the mean number of vesicles released per evoked action potential in control and *Rab8* mutants. We find a significant ($P < 2.5 \times 10^{-5}$) increase in the amount of vesicles released in *Rab8* mutants: the quantal content of *Rab8* mutant synapses is 61.3 ± 2.6 ($n = 21$), whereas it is 46.7 ± 1.4 in controls ($n = 22$). *Rab8* mutant animals rescued by neuronal expression of *Rab8* still show similar increase in vesicle release quantal content of 64.5 ± 3.9 ($n = 12$), indistinguishable from *Rab8* mutants ($P > 0.49$) and significantly different from control flies ($P < 8 \times 10^{-4}$). *Rab8* mutant animals rescued by muscle expression of *Rab8* show a mean quantal content of 52 ± 2.4 ($n = 11$) similar to wild-type values ($P > 0.07$) and significantly different from mutant values ($P < 0.02$). The values are means ± SEM. ***, $P < 0.001$; **, $P < 0.01$; *, $P < 0.05$.

intermediates observed in cortical neurons expressing *CHMP-2B*^{Intron5} (Lee et al., 2007) and are never observed in wild-type animals.

A Rab8-dependent process restricts TGF-β signaling

Disruption of endosomal traffic has been shown to be a major mechanism in the generation of synapse overgrowth driven by aberrant TGF-β signaling at the *Drosophila* NMJ (Sweeney and Davis, 2002; Wang et al., 2007; O'Connor-Giles et al., 2008; Rodal et al., 2011; Shi et al., 2013; Vanlandingham et al., 2013). We hypothesized that disruption of the endosome via loss of Rab8 would lead to misregulated TGF-β signaling. We therefore examined the role of TGF-β in the overgrowth of synapses in *Rab8* mutants.

Trans-heterozygous combinations of mutations in the TGF-β type-I receptor *thick veins* (*Tkv*) elicit a ∼50% reduction in synaptic bouton number, whereas loss of one copy of *Tkv* has no effect on bouton number (Fig. 5, A and B; Sweeney and Davis, 2002). When present in a *Rab8* mutant background, heterozygous and trans-heterozygous *Tkv* mutant combinations reduce synaptic overgrowth in a dose-dependent manner (Fig. 5, A and B). Although heterozygous mutations in *Rab8* or *Dad* (an inhibitory SMAD [Similar to Mothers Against Decapentaplegic] and negative regulator of TGF-β signaling; Tsuneizumi et al., 1997; Inoue et al., 1998) do not show any perturbation to synaptic bouton number, heterozygous combinations of *Rab8*^{1} and *Dad*$^{\Delta IEL}$ have an increased bouton number comparable to that of *Rab8* trans-heterozygotes (Fig. 5, A and B). A permissive TGF-β signal is essential for the synaptic overgrowth phenotype observed in *Rab8* mutants.

Next, we asked whether mutants showed misregulated TGF-β signaling in neurons. Upon ligand binding, TGF-β type II receptors recruit type-I receptors forming an active tetrameric complex (Massagué, 2012). Active receptors phosphorylate downstream receptor SMADs, which translocate to the nucleus. The *Drosophila* receptor SMAD is MAD (Mothers against decapentaplegic; Sekelsky et al., 1995), and levels of nuclear phosphorylated MAD (P-MAD) provide a reliable readout of TGF-β receptor activity. The levels of P-MAD are greatly elevated in Eve-positive motor neuron nuclei of *Rab8* mutant larvae (Fig. 5, C and D). In addition, the type II receptor, Wit, is more abundant in *Rab8* mutants compared with wild type (Fig. S4 C). As *Dad* is transcriptionally activated by TGF-β signaling, a *Dad-LacZ* enhancer trap can be used as a reporter of transcriptional TGF-β activity (Tsuneizumi et al., 1997). In *Rab8* mutants, levels of *Dad*-driven LacZ expression were elevated throughout the larval VNC (Fig. 5 E) and specifically within Eve-positive motor neuron nuclei (Fig. 5, E and F). These findings demonstrate synaptic overgrowth in *Rab8* mutants requires a permissive TGF-β signal, which is elevated at a signaling and transcriptional level in mutants and that Rab8 suppresses TGF-β signaling.

JNK acts synergistically with TGF-β to regulate synaptic growth in *Rab8* mutants

Previous studies demonstrated that the JNK–activator protein-1 (AP-1) signal transduction pathway plays a major role in the activation of overgrowth of the larval NMJ (Collins et al., 2006) gating the activity of the TGF-β pathway when synaptic growth is seen to be substantially above that of a wild-type synapse (Berke et al., 2013). In previous studies, genetic activation of TGF-β signaling alone at the larval NMJ has resulted in only modest increases in synapse growth (Sweeney and Davis, 2002; Rawson et al., 2003; McCabe et al., 2004; Berke et al., 2013). The JNK–AP-1 pathway has been identified as an evolutionarily conserved stress-activated kinase pathway that can be activated in response to a range of both endogenous and environmental stimuli in neurons. In response to stimuli, a kinase cascade, acting through JNK, activates a series of downstream targets, including

Published March 23, 2015

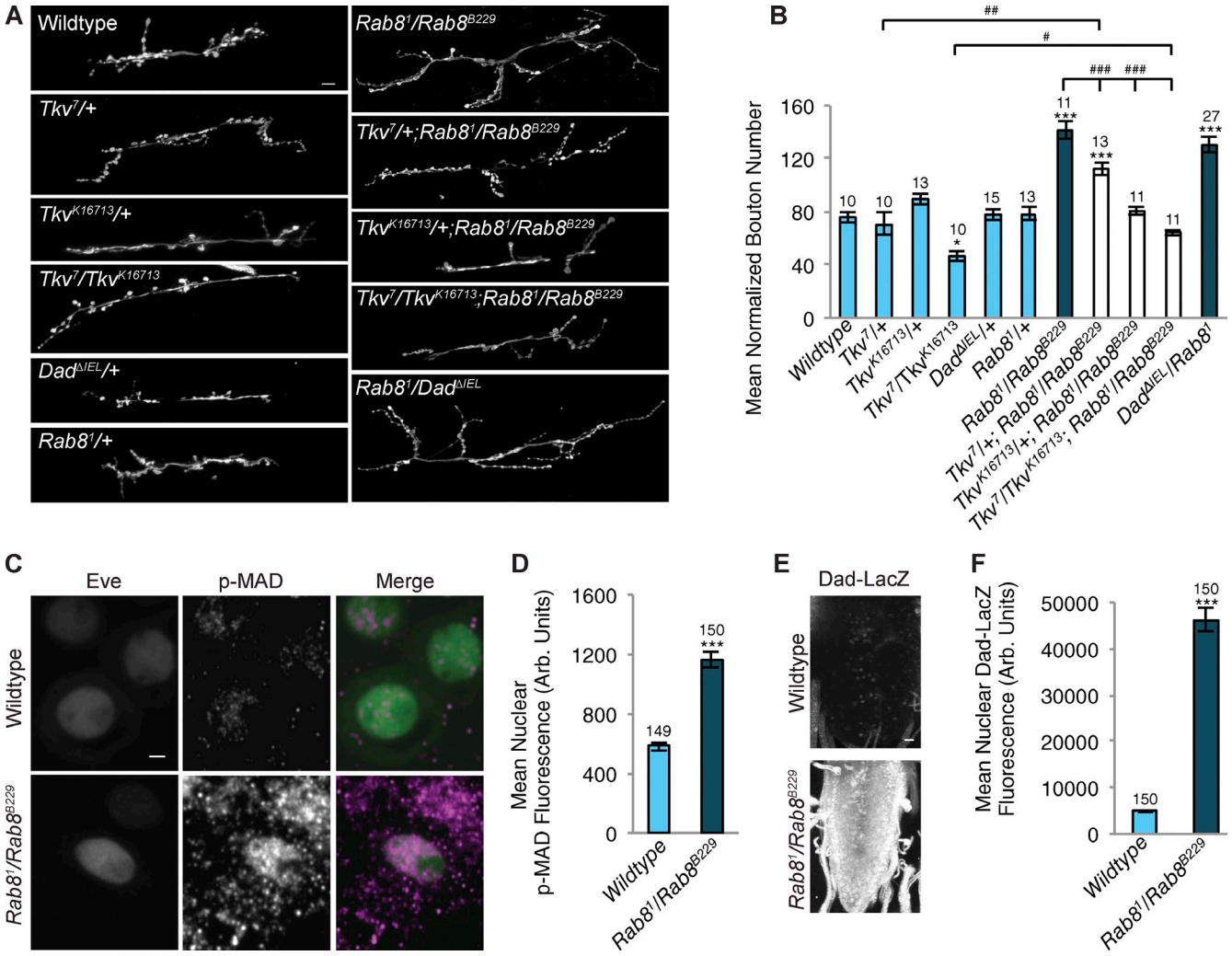

Figure 5. **Synaptic overgrowth in *Rab8* mutants requires a permissive and elevated TGF-β signal.** (A and B) Inhibition of TGF-β signaling through *thick veins* (*Tkv*) loss-of-function mutants alleviates synaptic overgrowth in a trans-heterozygous *Rab8* mutant background. Alleviating the inhibition of TGF-β signaling maintained by the inhibitory SMAD, Dad, using the loss-of-function mutant $Dad^{\Delta IEL}$ elicits no effect upon synaptic bouton number. $Dad^{\Delta IEL}/Rab8^{1}$ double-heterozygote combination shows synaptic overgrowth similar to *Rab8* trans-heterozygotes. ANOVA: F (d.f. 10) = 27.8476; P < 0.001 with post-hoc Dunnett's comparison to wild type: ***, P < 0.001; *, P < 0.05. Post-hoc Student's *t* test comparison between groups: ###, P < 0.001; ##, P < 0.01; #, P < 0.05. (C and D) *Rab8* mutants show significantly elevated levels of phospho-MAD, the activated form of the *Drosophila* receptor SMAD, within Eve-positive nuclei. ANOVA: F (d.f. 1) = 92.3468; ***, P < 0.001. (E and F) *Rab8* mutants show increased transcriptional activation of the TGF-β signaling pathway, with increased levels of *Dad*-driven LacZ expression within the VNC and within Eve-positive nuclei. ANOVA: F (d.f. 1) = 257.76; ***, P < 0.001. Arb. Units, arbitrary units. Numbers above bars = *n*. Error bars show SEM. Bars: (A and E) 10 µm; (C) 2 µm.

AP-1, comprised of hetero- and/or homo-dimers of Fos and Jun (Antoniou and Borsello, 2012). Expression of a dominant-negative Fos (Fos^{DN}) can be used to inhibit JNK/AP-1 signaling (Eresh et al., 1997; Collins et al., 2006). Neuronal expression of Fos^{DN}, under the control of the panneuronal driver *n-Syb*–Gal4 or motor neuron driver OK6-Gal4, does not affect NMJ growth in a wild-type background (Fig. 6, A and B). However, expression of Fos^{DN} both panneuronally and in motor neurons alone is sufficient to completely alleviate synaptic overgrowth in *Rab8* mutants (Fig. 6, A and B). In addition, although heterozygous mutants of *puc* (*puckered*), a negative regulator of JNK that is transcriptionally activated by JNK signaling, display no perturbation to NMJ size, heterozygous combinations of puc^{E69} and $Rab8^{1}$ have an increase in synaptic bouton number comparable to that seen in *Rab8* trans-heterozygote combinations (Fig. 6, A and B). We then asked whether AP-1 transcriptional activity was elevated in *Rab8* mutant neurons. *Puc* is a transcriptional target of AP-1 signaling (Martín-Blanco et al., 1998). Using a *Puc*-LacZ enhancer trap as a transcriptional reporter, we confirm the JNK–AP-1 signaling pathway to be more active in the motor neuronal nuclei of *Rab8* mutant larvae compared with wild type (Fig. 6, C and D). Collectively, this genetic evidence indicates JNK signaling to be essential for the synaptic overgrowth observed in *Rab8* mutants.

The endosomal JNK scaffold POSH acts as a nexus for regulation of synaptic overgrowth

The endosomal JNK scaffold and E3 ubiquitin ligase POSH plays a fundamental role in the regulation of JNK activity, mediating temporal activation and termination of a JNK signaling cascade (Xu et al., 2003, 2005; Kukekov et al., 2006) though

Published March 23, 2015

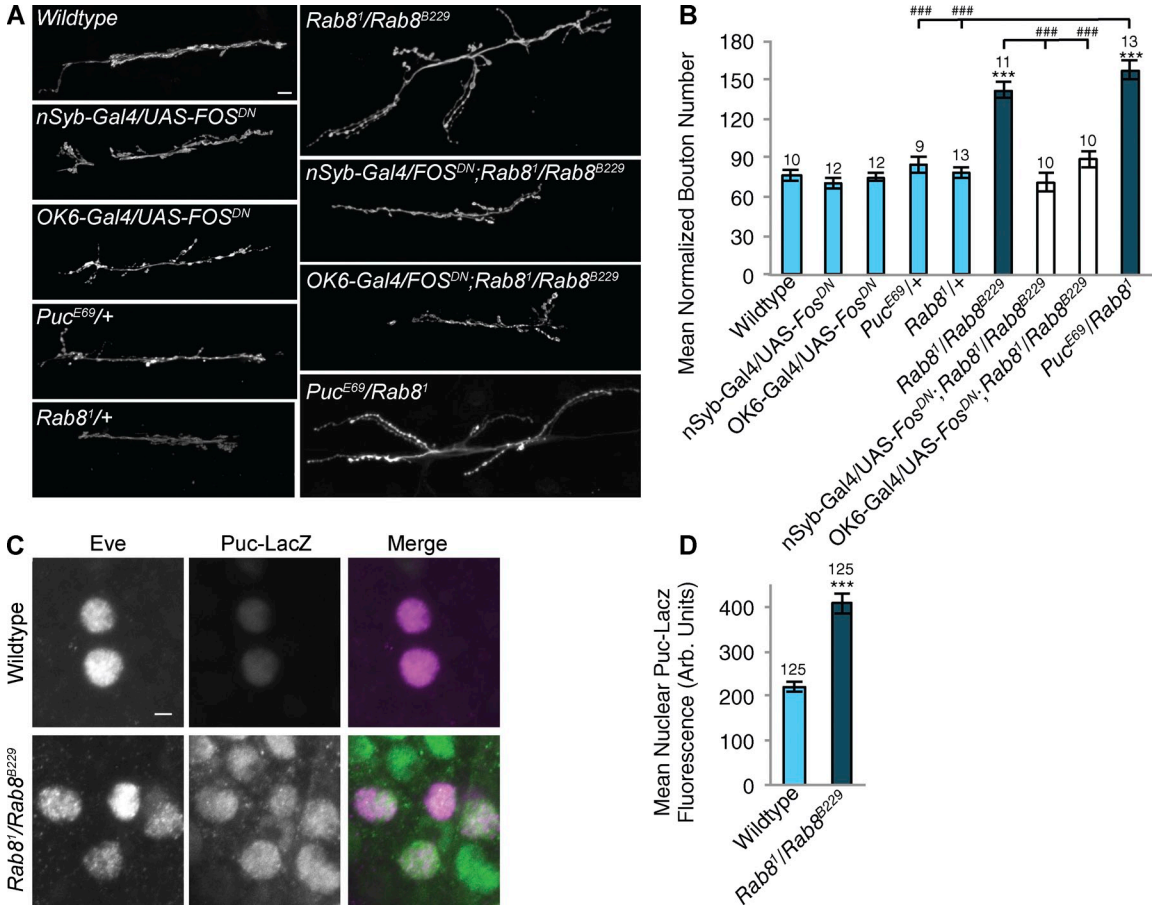

Figure 6. ***Rab8* mutants show elevated JNK signaling essential for synaptic overgrowth.** (A and B) Inhibition of the JNK signaling pathway by panneuronal (n-Syb–Gal4)– or motor neuronal (OK6-Gal4)–driven expression of a dominant-negative *Fos* construct, UAS-FOS^{DN}, in a *Rab8* mutant background completely rescues increased synaptic bouton number observed in *Rab8* mutants. Expression of Fos^{DN} in a wild-type background has no effect upon bouton number. Suppression of *puc*-mediated JNK inhibition through the presence of a heterozygous *puc* loss-of-function mutant (puc^{E69}) combined with heterozygous $Rab8^{1}$ induces synaptic overgrowth comparable to that seen in a *Rab8* trans-heterozygote mutant. Neither $Rab8^{1}$/+ or puc^{E69}/+ alone have any effect on bouton number. Bar, 10 µm. ANOVA: F(d.f. 8) = 36.4999; P < 0.001 with post-hoc Dunnett's comparison to wild-type controls: ***, P < 0.001. Student's *t* test comparison between genotypes: ###, P < 0.001. (C and D) *Rab8* mutants show significantly elevated levels of *puc*-driven LacZ expression in Eve-positive nuclei, indicating increased transcriptional activation of JNK signaling. Bar, 2 µm. ANOVA: F (d.f. 1) = 53.6294; ***, P < 0.001. Arb. Units, arbitrary units. Numbers above bars = *n*. Error bars show SEM.

function in the nervous system has been relatively unstudied to date (Zhang et al., 2005, 2006). An interaction between POSH and ESCRT-III, via ALG2 and AliX (Tsuda et al., 2006; Votteler et al., 2009), has been demonstrated. POSH also degrades HRS, via an E3 ubiquitin ligase activity (Kim et al., 2006).

Having observed perturbed endosomal dynamics, HRS depletion, and elevated JNK signaling in *Rab8* mutants, we asked whether POSH could provide a nexus linking these phenotypes with synaptic overgrowth. Here, we demonstrate an essential role for POSH in the regulation of synaptic growth in *Rab8* mutants. Introducing *POSH* mutants into a *Rab8* mutant background alleviates synaptic overgrowth (Fig. 7, A and B). Puncta of POSH, colocalizing with accumulations of P-MAD and the late endosomal marker spin (spinster; Sweeney and Davis, 2002) were observed in all larval axon bundles in *Rab8* mutants, a phenotype not observed in wild type (Fig. 7, C and D). P-MAD accumulations were reversed by the introduction of *POSH*-null mutants into a *Rab8* mutant background (Fig. 7, C and D). If POSH is acting as a scaffold for JNK–AP-1 signaling and regulator of HRS abundance in the motor neuron, we would predict that the introduction of *POSH*-null alleles into a *Rab8* mutant would prevent transcriptional activation of the *Puc-LacZ* reporter and HRS down-regulation. Examining *Puc*-driven LacZ expression in a *POSH/Rab8* mutant reduces transcriptional activation of the reporter dramatically compared with controls (Fig. 7 E). In addition, HRS levels are rescued to wild-type levels in a *POSH/Rab8* mutant (Fig. 7 F). HRS is known to regulate TGF-β signaling (Jékely and Rørth, 2003), so we asked whether *Dad*-LacZ and P-MAD abundance are also rescued in *POSH/Rab8* and we find that they are (Fig. 7, G and H). Overexpression of HRS in a *Rab8* mutant background rescues synaptic overgrowth (Fig. 8) consistent with HRS regulating synaptic overgrowth via TGF-β receptor degradation (Rodal et al., 2011).

A role for POSH and TAK1 in the regulation of synaptic growth

POSH scaffolds the JNKKK TAK1 to activate JNK signaling pathways during innate immune and proapoptotic responses in *Drosophila* (Tsuda et al., 2005; Lennox and Stronach, 2010). The E3 ubiquitin ligase activity of POSH has also been shown

Published March 23, 2015

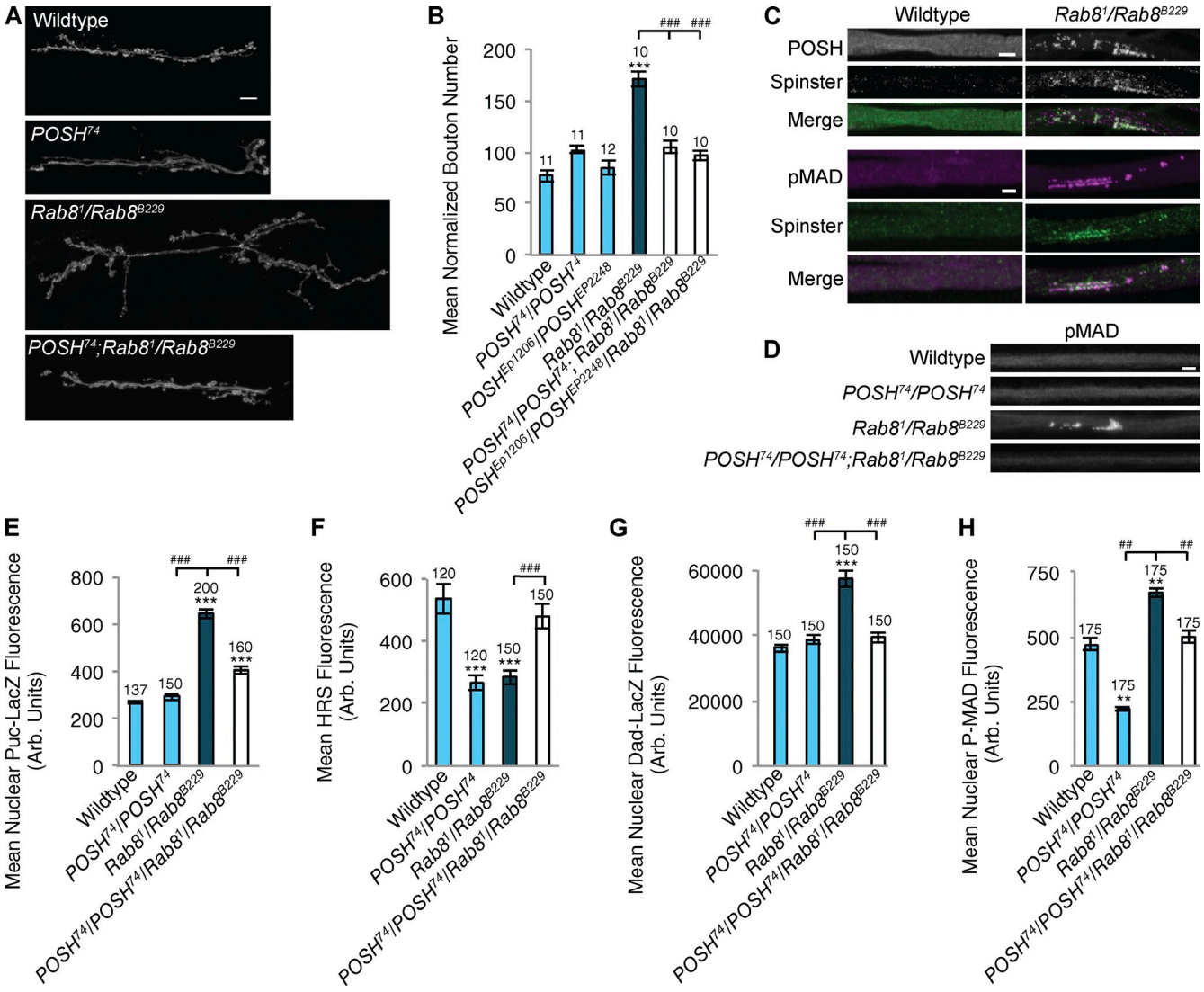

Figure 7. ***Rab8* mutants reveal a role for the endosomal JNK scaffold POSH in regulation of synaptic overgrowth at the NMJ.** (A and B) Increased synaptic bouton number in *Rab8* mutants can be alleviated through inhibition of POSH, using a homozygous *POSH*-null allele, $POSH^{74}$, or trans-heterozygous $POSH^{EP1206}/POSH^{EP2248}$ loss-of-function mutants in a *Rab8* mutant background. ANOVA: F(d.f.5) = 28.149; P < 0.001), with post-hoc Dunnett's comparison to wild-type control: ***, P < 0.001. Student's *t* test comparison between genotypes: ###, P < 0.001. (ANOVA: F(d.f.5) = 28.149; P < 0.001). (C) Immunohistochemical staining reveals POSH accumulations colocalizing with the late endosomal marker spin and P-MAD in axons of trans-heterozygous *Rab8* mutant larvae. Accumulations of spin, POSH, or P-MAD were never observed in wild-type axons. POSH colocalizes with spin PCC: 0.74 ± 0.03; MCC M1: 0.98 ± 0.013; M2: 0.91 ± 0.014; *n* = 12. P-MAD colocalizes with spin PCC: 0.63 ± 0.027; MCC M1: 0.93 ± 0.020; M2: 0.87 ± 0.024. (D) Loss of *POSH* in a *Rab8* mutant background alleviates axonal aggregates. P-MAD is used as a representative marker of aggregates. (E–H) Loss of *POSH* rescues elevated *Puc*-lacZ (E), depleted HRS (F), elevated *Dad*-LacZ (G), and P-MAD (H) levels observed in *Rab8* mutants. (E) ANOVA: F(d.f.3) = 105.553; P < 0.001. (F) ANOVA: F(d.f.3) = 9.921; P < 0.001. (G) ANOVA: F(d.f.3) = 33.205; P < 0.001. (H) ANOVA: F(d.f.3) = 93.205; P < 0.001, with post-hoc Dunnett's comparison to wild-type controls: ***, P < 0.001; **, P < 0.01. Student's *t* test comparison between genotypes: ###, P < 0.001; ##, P < 0.01. Arb. Units, arbitrary units. Numbers above bars = *n*. Error bars show SEM. Bars: (A) 10 µm; (C and D) 5 µm.

to be essential for triggering the proteasomal degradation of TAK1 to limit activation of NF-κB and JNK during immune responses (Tsuda et al., 2005). TAK1 was originally identified as a TGF-β–activated kinase (Yamaguchi et al., 1995), providing a possible bridge between TGF-β and JNK signaling in the regulation of synaptic growth. We asked whether TAK1 was essential for synaptic overgrowth observed in *Rab8* mutants. Although heterozygous *TAK1* loss-of-function mutants and neuronal expression of a dominant-negative TAK1 or TAK1-RNAi have no effect upon synaptic bouton number alone they are sufficient to alleviate overgrowth in a *Rab8* mutant background (Fig. 8). Neuronal overexpression of UAS-*TAK1* also elicited a significant synaptic overgrowth phenotype, with an expanded synapse consisting of several very small boutons (Fig. 8).

Rab8 expression rescues synaptic growth parameters caused by $CHMP2B^{Intron5}$ misexpression in motor neurons

We have shown Rab8 to be a component of the recycling endosome at the synapse, whereas CHMP2B functions at the MVB. Previously, Rodal et al. (2011) showed that recycling endosome function repressed synaptic growth, in conjunction with the

Published March 23, 2015

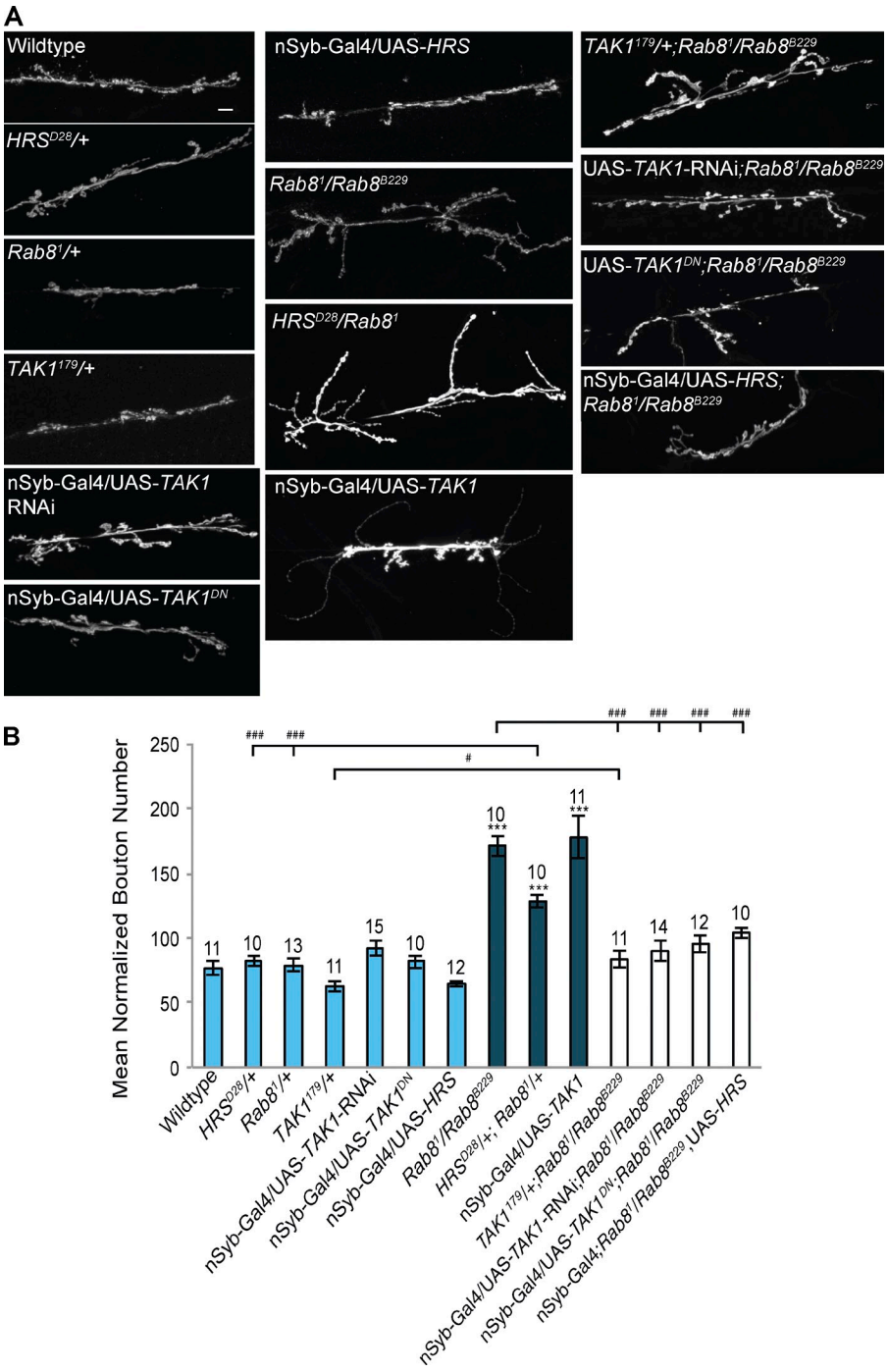

Figure 8. ***Rab8* mutants reveal a role for the JNKKK TAK1 in synaptic overgrowth at the NMJ.** (A and B) Loss of TAK1 function generated by Inhibition of *TAK1* through panneuronal (n-Syb–Gal4) expression of a dominant-negative form of *TAK1*, knockdown by *TAK1*-RNAi, or use of a *TAK1* loss-of-function allele completely alleviated synaptic overgrowth in a *Rab8* mutant background. Correspondingly panneuronal expression of UAS-*TAK1* promotes synaptic overgrowth, characterized by a significant increase in synaptic bouton number. Reduction of *HRS* function, using a heterozygous *HRS* loss-of-function allele $HRS^{D28}/+$, in combination with $Rab8^{1}/+$ elicited a significant increase in synaptic bouton number. $HRS^{D28}/+$ or $Rab8^{1}/+$ alone did not affect bouton number. Bar, 10 µm. ANOVA: $F(d.f.\ 11) = 24.2733$; $P < 0.001$ with post-hoc Dunnett's comparison to wild-type control: ***, $P < 0.001$. Student's *t* test comparison between genotypes: ###, $P < 0.001$; #, $P < 0.05$. Numbers above bars = *n*. Error bars show SEM.

MVB. We hypothesized that Rab8/recycling endosome function could rescue synaptic overgrowth by repressing TGF-β function when MVB function was compromised by $CHMP2B^{Intron5}$ expression. Overexpressing $CHMP2B^{Intron5}$ in motor neurons induced a 30% increase in synaptic growth in addition to increases in P-MAD abundance, *Dad*-LacZ and *Puc*-LacZ reporter induction and accumulations of the ESCRT-III protein, Shrub, colocalizing with Wit and the late endosomal marker spin (Fig. 9, A–F). All of these cellular deficits and synaptic growth parameters were reversed to wild-type levels when Rab8 was coexpressed with $CHMP2B^{Intron5}$ in motor neurons (Fig. 9, A–E; and Fig. S5). We then asked whether $CHMP2B^{Intron5}$ accumulation in mammalian neurons could induce POSH association. Expression of FLAG-tagged $CHMP2B^{Intron5}$ in mouse primary cortical neurons generated puncta of colocalizing mPOSH in neurites (Fig. 9 G), suggesting association between these two proteins can occur in neurons with dysfunctional ESCRT-III activity.

Discussion

Endosomal function, synaptic growth, and neurodegeneration

By regulating the temporal and spatial distribution of cell membrane receptors, endosomal trafficking plays a critical role in

Published March 23, 2015

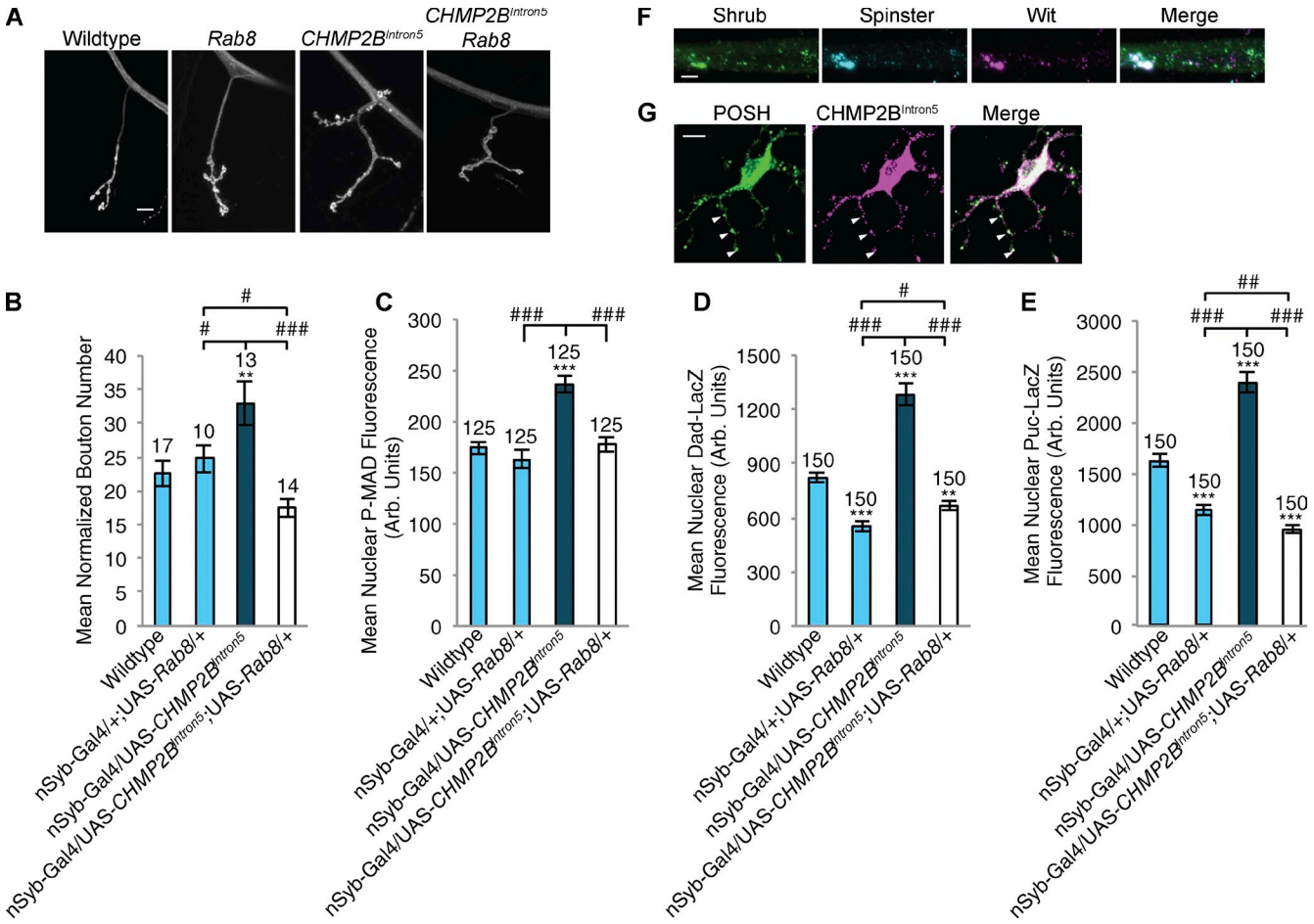

Figure 9. **Synaptic overgrowth and associated up-regulated markers induced by *CHMP2B*^{Intron5} expression are alleviated by *Rab8* expression.** (A and B) Panneuronal (n-Syb–Gal4) expression of the UAS-*CHMP2B*^{Intron5} mutant transgene elicited significant synaptic overgrowth, muscle 4 hemisegment A3. Overgrowth was rescued by coexpression of UAS-*Rab8*. ANOVA: F(d.f. 3) = 25.2705; P < 0.001 with post-hoc Dunnett's comparison to wild-type control: **, P < 0.01. Post-hoc Student's *t* test comparison between groups: ###, P < 0.001; #, P < 0.05. (C–E) Panneuronal (n-Syb–Gal4) expression of the UAS-*CHMP2B*^{Intron5} mutant transgene elicited a significant increase in nuclear P-MAD (C), *Dad*-LacZ (D), and *Puc*-LacZ (E) within Eve-positive motor neuron nuclei. In all cases, coexpression of UAS-*Rab8* was sufficient to rescue to wild-type levels. (C) ANOVA: F (d.f. 3) = 18.873; P < 0.001. (D) ANOVA: F (d.f. 3) = 77.984; P < 0.001. (E) ANOVA: F (d.f. 3) = 93.059; P < 0.001 with post-hoc Dunnett's comparison to wild type controls: ***, P < 0.001; **, P < 0.01. Post-hoc Student *t* test comparison between groups: ###, P < 0.001; ##, P < 0.01; #, P < 0.05. (F) Panneuronal (n-Syb–Gal4) expression of the UAS-*CHMP2B*^{Intron5} mutant transgene induced accumulation of the ESCRT-III component Shrub in axons. Accumulations colocalized with both spin and Wit. Aggregates were not observed in wild-type animals. (G) Mouse primary cortical neurons transfected with *CHMP2B*^{Intron5} show CHMP2B^{Intron5} aggregates colocalizing with POSH within neuronal projections. Arrowheads denote points of colocalization between POSH and CHMP2B^{Intron5}. Numbers above bars = *n*. Error bars show SEM. Bars: (A and G) 10 µm; (F) 5 µm.

modulating signaling within cells (Seto et al., 2002). This process is essential for neuronal function and plasticity with endosomal perturbation contributing to a range of pathologies, including lysosomal storage disorders (Sweeney and Davis, 2002; Fukuda et al., 2006) and spastic paraplegia (Wang et al., 2007). Why distinct populations of neurons are sensitive to disruption in endosomal function is not clear. Regulation of TGF-β signaling has been shown to play a fundamental role in synapse development and function, centrally and at the NMJ, in both vertebrate and invertebrate species (Baines, 2004; Marqués, 2005; Xiao et al., 2013). At the *Drosophila* larval NMJ, a retrograde TGF-β signal, secreted by the muscle and synaptic glia, regulates a program of synaptic growth and plasticity within the growing motor neuron (Sweeney and Davis, 2002; McCabe et al., 2003; Rawson et al., 2003; Fuentes-Medel et al., 2012; Berke et al., 2013). This process is reliant upon the endocytic machinery with ligand-bound TGF-β receptors endocytosed, in an activity-dependent manner, at the NMJ and translocated retrogradely to the motor neuron cell body, to convey the signal (Smith et al., 2012). Rodal et al. (2011) demonstrated that TGF-β signaling is particularly sensitive to perturbations in endocytic trafficking of receptors either through the MVB or recycling endosome. Disruption of both endosomal compartments resulted in significant synaptic overgrowth via up-regulated TGF-β signaling at the larval NMJ. Overgrowth of the larval NMJ is codependent on activation of the JNK–AP-1 pathway (Berke et al., 2013). Interestingly, mutants identified with a doubling of synaptic size (in the range of *Rab8* mutants), *spinster* and *highwire* (*Hiw*), are both associated with neurodegeneration (Wan et al., 2000; Sweeney and Davis 2002). Here, we support and expand these findings by identifying Rab8 as a novel regulator of a neurodegenerative phenotype and synaptic growth.

Published March 23, 2015

The recycling endosome and regulation of synaptic growth

We identify Rab8 as a dominant modifier of a neurodegenerative phenotype caused by expression of the FTD-associated CHMP-2B^{Intron5} protein. Rab8 is known to be localized and to regulate function of the recycling endosome (Ang et al., 2003; Sato et al., 2007). Rab8 mutants show a synaptic overgrowth of ~100%, induced by dysregulation of TGF-β and JNK signaling in the synapse. We show that loss of Rab8 function in *Drosophila* generates reduction of Rab4 and Rab11 proteins associated with the recycling endosome and suppression of TGF-β signaling at the *Drosophila* NMJ (Rodal et al., 2011). In *Rab8* mutants, presynaptic membrane structures are seen bearing a strong resemblance to those observed in mutants with early endosome dysfunction (Zhang et al., 1998; Shimizu et al., 2003; Kasprowicz et al., 2008; Kawasaki et al., 2011; Winther et al., 2013), potentially increasing opportunity for TGF-β signaling before sequestration and signaling repression by the MVB or recycling endosome. Loss of Rab8 activates POSH, which reduces abundance of the ESCRT-0 protein HRS, known to directly regulate the abundance of TGF-β receptors (Jékely and Rørth, 2003; Kim et al., 2006) through its role in promoting MVB formation. We suggest that the loss of recycling endosome function and degradative traffic into the MVB in *Rab8* mutants results in an abundance of the TGF-β effector P-SMAD, contributing to synaptic growth. We support this observation by the rescue of synaptic overgrowth via the overexpression of HRS in motor neurons in *Rab8* mutants (Fig. 8). We also observe that Rab8 expression, presumably by increasing recycling endosome function and suppression of TGF-β activity, reverses all aspects of synaptic growth activation induced by expression of the CHMP2B^{Intron5} protein. Rab8 appears to act upstream of Rab11. Overexpression of Rab11 in a *Rab8* mutant background rescues synaptic overgrowth (Fig. S3, D and E). These findings point to the critical function of recycling endosome function in allowing appropriate synaptic growth when MVB activity is compromised by the FTD associated CHMP2B^{Intron5} protein.

Regulators of synaptic growth, POSH and TAK1, provide a novel mechanism for cross talk between TGF-β and JNK signaling

Previous studies have shown that, in other contexts, TGF-β and JNK signaling show direct and mutual interaction (Yamaguchi et al., 1995; Perlman et al., 2001; Mao et al., 2011). TGF-β is capable of activating JNK in a SMAD-independent, TAK1-dependent manner (Sorrentino et al., 2008). Conversely, it has been shown that JNK signaling can activate TGF-β, with AP-1 components directly interacting with SMADs and JNK regulating TGF-β (Engel et al., 1999; Derynck and Zhang, 2003). The observations made here provide evidence of a similar mechanism of cross talk within neurons, with synaptic overgrowth requiring synergistic TGF-β and JNK activity as well as being TAK1 dependent.

We have shown that *Rab8* mutants show endosomal dysfunction and aberrant accumulations of POSH within axon bundles projecting from the larval VNC. POSH has previously been identified as an endosomal JNK scaffold as well as a regulator of TAK1 abundance and TAK1-mediated JNK signaling (Tsuda et al., 2005; Lennox and Stronach, 2010). We propose that POSH accumulates on aberrant endosomes (Tsuda et al., 2006; Votteler et al., 2009) and is likely to elicit ectopic activation of the JNK cascade, explaining the elevated JNK signaling observed in *Rab8* mutants. It has been shown that the JNK–AP-1 pathway is involved in regulating synaptic growth and plasticity at the *Drosophila* NMJ (Sanyal et al., 2002; Collins et al., 2006; Milton et al., 2011). For example, larvae with mutations in the E3 ubiquitin ligase *Hiw* show synaptic overgrowth associated with a reduction in *Hiw*-mediated degradation of the JNKKK Wnd (Wallenda; Collins et al., 2006). In the *Hiw* mutant, absence of the E3 ubiquitin ligase activity of the Hiw protein leads to failure to degrade the JNKKK Wnd, which then drives synaptic overgrowth (Collins et al., 2006). We asked whether POSH was required to scaffold Wnd to drive synaptic overgrowth in the *Hiw* mutant by generating a *Hiw/POSH* double mutant. We found that POSH mutations do not suppress the *Hiw* phenotype, indicating no requirement for POSH in *Hiw*-driven overgrowth (Fig. S4, A and B). In addition previous work in our laboratory has shown JNK signaling, activated by the JNKKK apoptosis signal-regulating kinase, elicits synaptic growth in response to oxidative stress (Milton et al., 2011). In this study, we identify TAK1, potentially acting through POSH, as a novel JNKKK regulating synaptic growth processes. It has been previously observed that reducing POSH or TAK1 function protects neurons against cell death in ischemia (Zhang et al., 2005, 2006; Neubert et al., 2011). These findings suggest that the JNK–AP-1 pathway acts as a master regulator of synaptic growth plasticity, responding to disparate endogenous and external cues through activation of different JNKKKs.

The Hiw protein has been shown to interact with the co-SMAD medea, but the functional significance of this interaction in regulating synapse overgrowth is unclear (McCabe et al., 2004). Our data describing POSH regulation of HRS to regulate TGF-β at the synapse further support a role for POSH as a nexus for regulation of both the TGF-β and JNK growth signals from the endosome during synaptic overgrowth at the *Drosophila* larval NMJ.

We observed only mild deficits in the synaptic release properties of the overgrown *Rab8* mutant synapse. We found that quantal size is significantly reduced in *Rab8* mutant synapses and that this defect is rescued by expression of Rab8 in the muscle (Fig. 4). This suggests that Rab8 may be involved in the glutamate receptor delivery at the *Drosophila* NMJ, a role described in mammalian dendritic spines where Rab8 is involved in the delivery of a-amino-3-hydroxy-5-methyl-4-isoxazolepropionic acid receptor and the control of synaptic function and plasticity (Gerges et al., 2004). In addition, our data show that *Rab8* mutant synapses can perform homeostatic compensation to decreased quantal size; mutant synapses and synapses rescued by neuronal Rab8 show increased quantal content (Fig. 4). In previously identified synaptic overgrowth mutants, synaptic function is decoupled from growth, and impaired synaptic output is observed (Sweeney and Davis, 2002; Collins et al., 2006; Milton et al., 2011). Activation of AP-1 (Fos and Jun) signaling in motor

Published March 23, 2015

neurons has been seen to increase synaptic function (Sanyal et al., 2002), whereas reduction of AP-1 activity in an overgrown synapse can rescue synaptic fatigue upon high frequency stimulation (Milton et al., 2011). Activity of the TGF-β effector, P-SMAD, is essential for synaptic growth homeostasis during development (McCabe et al., 2003), and is required to maintain synaptic output during growth (Goold and Davis, 2007). However, a comprehensive analysis of temporal and genetic requirements for P-SMAD signaling in conjunction with several synaptic growth signals (Berke et al., 2013) strongly suggests that P-SMAD activity is essential for activity-dependent growth plasticity and may be a major limiting factor for synaptic output during growth. In our *Rab8* mutants, we observed an excess of P-SMAD in addition to increased JNK–AP-1 activity, suggesting that neither are limiting for synaptic growth or activity.

Implications for our understanding of FTD

The identification of *Rab8* mutants as strong modifiers of the CHMP2B^{Intron5} eye phenotype led us to examine the role of Rab8 in NMJ growth and function. Both loss of Rab8 and expression of CHMP2B^{Intron5} in motor neurons cause enhanced synaptic growth and an increase of P-SMAD. Coexpression of *Rab8* reverses the increase in P-SMAD and synaptic overgrowth caused by CHMP2B^{Intron5}. ESCRT-III complexes are known to fail to dissociate in the presence of CHMP2B^{Intron5} (Lee et al., 2007) and have the potential to promote association with POSH through the interaction of ALiX and Alg-2 (Tsuda et al., 2006; Votteler et al., 2009). We show that POSH accumulates on CHMP2B^{Intron5}-positive puncta within neurites in mouse primary cortical neurons expressing CHMP2B^{Intron5} (Fig. 9 G). The presence of CHMP2B^{Intron5} mutations in FTD may therefore lead to enhanced signaling via TAK1 and POSH contributing to synapse growth misregulation and eventual cell death. Indeed, dendritic spine abnormalities and synaptic defects are observed in a mouse model of FTD expressing CHMP2B^{Intron5} (Gascon et al., 2014). It is conceivable that such events could contribute to cognitive dysfunction and neuronal death in FTD.

Materials and methods

Fly stocks and maintenance

Drosophila strains were raised on a standard yeast, sugar, and agar medium at 25°C. Canton-S outcrossed to w^{1118} flies were used as wild-type controls. UAS-*CHMP2B*^{Intron5} flies were described previously (Ahmad et al., 2009). Stocks were obtained from the following sources: *GMR*-Gal4 (Freeman, 1996); *MHC*-Gal4 (Davis et al., 1997); *Df(3L)ED228* (Ryder et al., 2007); *Rab8*^{1} (Giagtzoglou et al., 2012); PBac{5HPw^{+}}*Rab8*^{B229}, UAS-*mCD8*-GFP, *actin*(5c)-Gal4, and P{*LacW*}*Dad*^{J1E4} (Tsuneizumi et al., 1997); UAS-*FOS*^{DN} (a dominant-negative construct expressing the bZip domain of dFos; Eresh et al., 1997); P{*LacZ*}*Puc*^{E69} (Martín-Blanco et al., 1998); *POSH*^{EP1206} and *POSH*^{EP2248} (Tsuda et al., 2005); *TAK1*^{179} (Delaney et al., 2006); UAS-CA-*Rab8*-YFP (a Q67L mutation in the *Rab8* open reading frame; Zhang et al., 2007); UAS-*Rab11-EGFP* and UAS-*Rab4-RFP* (Bloomington *Drosophila* Stock Center); *Rab8*^{2}, *Rab8*^{3}, and *Rab8*^{Z3007} (J. Kennison, National Institutes of Health, Bethesda, MD); UAS-*POSH* and *POSH*^{74} (a null allele of POSH; Tsuda et al., 2005); UAS-LAMP-EGFP (Pulipparacharuvil et al., 2005); UAS-*TAK1*, UAS-*TAK1-RNAi*, and UAS-*TAK1*^{K46R} (Mihaly et al., 2001); *HRS*^{D28} (Lloyd et al., 2002); *OK6*-Gal4 (Sanyal 2009); *n-Syb*–Gal4 (Pauli et al., 2008); *Rab8*-Gal4 (Chan et al., 2011); and *Hiw*^{ND9} (Wan et al., 2000).

Generation of transgenic stocks

UAS-*Rab8* stocks were generated through subcloning of the *Rab8* cDNA (LD44762; Berkeley Drosophila Genome Project, Gold Collection) into a pUASt vector and microinjected into w^{1118} wild-type embryos. UAS-Rab8-RNAi was constructed using the pWIZ vector (Lee and Carthew, 2003) using the following oligonucleotides: Rab85′, 5′-CGCTCTAGACTCG-AGTGGGCTGTTTTACACTTTTGG-3′, and Rab83′, 5′-CGCTCTAGACT-GTTAGGTTCGAGTACAAGCG-3′.

Genetic interaction studies

Genetic interaction experiments and quantification of the *CHMP2B*^{Intron5} eye phenotype was performed as described in Ahmad et al. (2009) and Lu et al. (2013). Flies of the genotype *GMR-GAL4, UAS-CHMP2B*^{Intron5}*/CyO* were to crossed deficiency and mutant stocks described in Fig. 1. Melanization of eyes from resulting offspring was scored as low, medium, or high. Eyes were imaged using a camera (AxioCam ERc 5s; Carl Zeiss) on a dissecting scope (Stemi 2000-C; Carl Zeiss).

Immunohistochemistry

Third instar wandering larvae were dissected in PBS, fixed in 3.7% formaldehyde/PBS for 7 min, and stained using the appropriate primary antibodies. Primary antibodies were used at the following concentrations: mouse anti-Eve (1:50; 3C10; Developmental Studies Hybridoma Bank [DSHB]), anti-Wit (1:5; 23C7; DSHB), rabbit anti-pMAD (PS1, raised to a peptide KKKNPISSVS, containing two C-terminal phosphoserine residues representing the phosphorylated tail of Smad1; 1:500; Persson et al., 1998), rabbit anti-Rab11 (raised to a peptide CSQKQIRDPPEGDVI representing amino acid residues 177–191 of Rab11; 1:8,000; Tanaka and Nakamura, 2008), guinea pig anti-HRS (raised to an N-terminal domain of HRS fused to GST; 1:200; Lloyd et al., 2002), guinea pig anti-Spin (raised to two coinjected peptides encoding the N-terminal 7-kD soluble sequence before the first transmembrane domain, and a 9-kD sequence encoding the soluble region between transmembrane domains 11 and 12 of Spin; 1:1,000; Sweeney and Davis, 2002), mouse anti–mitochondrial complex V (1:1,000; 15H4C4; Abcam), rabbit anti-dPOSH (raised to a GST-POSH fusion protein; 1:20; Tsuda et al., 2005), rabbit anti-Shrub (raised to a shrub-GST fusion protein; 1:500; Sweeney et al., 2006), rabbit anti–β-galactosidase (1:1,000; Cappel Laboratories), and Cy3-conjugated anti-HRP (1:200; Stratech Scientific). Rabbit anti-synaptotagmin (1:2,000) was raised in the following manner: a cDNA encoding dSyt1 was obtained from I. Robinson (University of Plymouth, Plymouth, England, UK; Robinson et al., 2002). A Sal1–Xho1 fragment containing the lumenal soluble domains of dSyt1 was subcloned into the Sal1 site of the expression vector pGEX-4T-3. The GST-dSyt1 fusion protein was expressed in BL21 *Escherichia coli* and purified by standard methods. Fusion protein was injected into rabbits using a 3-mo immunization protocol by Eurogentec. Larval preparations were mounted in Vectashield mounting media. Control larvae were stained in the same solutions as experimental larvae.

Mammalian cell culture, transfection, and immunofluorescence

Primary neuronal cultures were obtained from C57/B6 mice (embryonic day 18). Cortex was dissected, trypsinized, and dissociated into single cells and plated in 12-well plates with coverslips in plating medium (DMEM and 10% FBS) for 4 h and then maintenance medium for 1–2 wk (Neurobasal medium, B27, and Glutamine). Cultures were maintained in a humidified incubator at 37°C and 5% CO_2. Plasmid pcDNA3.1-Flag-CHMP2B^{Intron5} was transiently transfected into cells with Lipofectamine 2000, as recommended by the manufacturer. Cells were fixed with 4% paraformaldehyde at room temperature for 10 min, washed three times with PBS, and blocked for 1 h at room temperature with 10% normal goat serum (Sigma-Aldrich) diluted in PBS containing 0.1% Triton X-100 (PBS-T) and 2% BSA (Sigma-Aldrich). Cells were incubated overnight at 4°C with primary antibodies (mouse anti-Flag; 1:200; Sigma-Aldrich) and rabbit anti-mPOSH (1:200; Proteintech). After three washes in PBS (10 min each), cells were incubated for 1 h at room temperature with secondary antibodies (goat anti–rabbit Alexa Fluor 488 and goat anti–mouse Alexa Fluor 594, both 1:1,000; Invitrogen) diluted in PBS. Cells were washed three times in PBS and mounted with Vectashield (Vector Laboratories).

Imaging and quantification

Synaptic bouton numbers at muscles 6/7 and 4, hemisegment A3, were determined by counting each distinct, spherical, anti-synaptotagmin–positive varicosity contacting the muscle. As synaptic bouton number has been shown to increase proportionally with muscle surface area synaptic bouton numbers were normalized against muscle surface area by dividing the bouton number by the muscle surface area and multiplying by mean wild-type muscle surface area as described by Milton et al. (2011). Muscles and synapses were imaged at room temperature using a camera (AxioCam HRC) on an inverted fluorescence microscope (Axiovert 200; Carl Zeiss)

using Plan Neofluar 10×/0.3 NA and 40×/0.75 NA lenses, with AxioVision Rel. 4.8 software (Carl Zeiss). Measurements were made from images using ImageJ (National Institutes of Health).

Confocal images were obtained using a confocal microscope (LSM 710 Axio Observer Z1; Carl Zeiss). Z-stacked images of single NMJ's were obtained using a Plan Apochromat 63×/1.4 NA oil objective. Z-stack projections of muscle 4 NMJ's were analyzed using ImageJ to quantify bouton diameter, NMJ length, and satellite bouton number. Bouton diameter was measured as the width across a bouton at the widest point (Milton et al., 2011). NMJ length was measured using the NeuronJ ImageJ plugin. Satellite boutons were defined as small supernumerary boutons budding from a central parent bouton (Marie et al., 2004). Larval VNC's were imaged using a Plan Neofluar 40×/1.3 NA oil objective. Axon bundles were imaged using a 63× oil objective. Motor neuron cell bodies were imaged using a 63× oil objective. The same settings were maintained for wild-type and experimental images. Mean nuclear LacZ fluorescence and cellular HRS fluorescence was calculated as corrected total fluorescence (integrated density − [area of nucleus/cell × mean fluorescence of background]). Rab4-RFP and Rab11-GFP fluorescence was quantified at the NMJ and normalized against a control channel (anti-HRP). Mouse neuronal cultures were examined with a confocal microscope (D-Eclipse; Nikon) using a 40× oil objective (NA 1.30) and EZC1 acquisition and analysis software (Nikon). For colocalization analysis, Pearson's correlation coefficient (PCC) and Manders overlap coefficient (M1 and M2) were calculated using Coloc2 plugin for Fiji, after background subtraction (rolling ball radius, 50 pixels).

Transmission EM

Third instar wandering larvae were dissected and fixed in 0.1 M $NaPO_4$, pH 7.4, 1% glutaraldehyde, and 4% formaldehyde, pH 7.3, overnight. Fixed larval preparations were washed 3× in 0.1 M $NaPO_4$ before incubation in OsO_4 (1% in 0.1 M $NaPO_4$; 2 h). Preparations were washed 3× in distilled water before incubation in 1% uranyl acetate. Preparations were washed (3× distilled water) and dehydrated through a graded ethanol series; 20% increments starting at 30% followed by two 100% changes and then 2× 100% propylene oxide. Preps were incubated in a graded series of epon araldite resin (in propylene oxide); 25% increments culminating in 3× 100% changes. Individual muscles and the VNC were then dissected out. These were then transferred into embedding molds, and the resin was polymerized at 60°C for 48 h. Resin mounted preps were sectioned (60–70 nm) using glass knives upon a microtome (Ultracut UCT; Leica) and placed onto grids. Preps were subsequently incubated in uranyl acetate (50% in ethanol), washed in distilled water, and incubated in lead citrate. Sections were imaged using a transmission electron microscope (TECNAI 12 G^2; FEI) with a camera (Soft Imaging Solutions MegaView; Olympus) and Tecnai user interface v2.1.8 and analySIS v3.2 (Soft Imaging Systems).

Electrophysiology

Recordings were performed as described previously (Maldonado et al., 2013). Specifically, wandering third-instar larvae were selected and were recorded in HL3 saline (70 mM NaCl, 5 mM KCl, 10 mM $NaHCO_3$, 115 mM sucrose, 5 mM trehalose, and 5 mM Hepes) with 0.4 mM Ca^{2+} and 10 mM Mg^{2+}. Muscle recordings were made from muscle 6 in abdominal segment 3 (A3) and were achieved using sharp electrodes (10–18 MΩ) filled with 3 M potassium chloride. Only the recordings with resting membrane potentials inferior to −60 mV and with input resistances greater than 5 MΩ were selected for the analysis. The mean miniature excitatory postsynaptic potential (EPSP; mEPSP) amplitude was quantified by measuring the amplitude of 100–200 individual sequential spontaneous mEPSP events per NMJ, using Mini Analysis software (Synaptosoft). The mean per NMJ mEPSP amplitudes were then calculated for each genotype. Stimulation threshold was set for each recording such that the maximal EPSP was achieved, recruiting both motoneurons innervating muscle 6. The mean of 20 suprathreshold evoked EPSP amplitude (stimulation at 0.5 Hz) was calculated for each synapse. Quantal content was calculated by dividing the mean maximal EPSP amplitude by the mean amplitude of the spontaneous miniature release events (mEPSP) for each recording and then averaged across synapses to generate the mean quantal content for each genotype.

Online supplemental material

Fig. S1 shows the mapping of point mutations identified in *Rab8* mutants, the genetic noncomplementation of the *Rab8* alleles, and the rescue of the *GMR-GAL4, UAS-CHMP2B^{Intron5}* eye phenotype by coexpression of UAS-*Rab8*. Fig. S2 describes the growth parameters of *Rab8* mutant NMJs. Fig. S3 shows the depletion of recycling endosome markers at *Rab8* mutant synapses and a rescue of the *Rab8* NMJ overgrowth phenotype by the overexpression of Rab11. Fig. S4 shows that *Hiw* NMJ overgrowth cannot be rescued by the introduction of POSH mutants into the *Hiw* genetic background and that there are no axonal trafficking defects for TGF-β receptor, synaptotagmin, or mitochondria in *Rab8* mutants. Fig. S5 shows the synaptic growth parameters for NMJs overexpressing *UAS-CHMP2B^{Intron5}* and their rescue by coexpression of UAS-*Rab8*. Online supplemental material is available at http://www.jcb.org/cgi/content/full/jcb.201404066/DC1. Additional data are available in the JCB DataViewer at http://dx.doi.org/10.1083/jcb.201404066.dv.

We thank the Bloomington *Drosophila* stock center, Developmental Studies Hybridoma Bank Iowa, the University of Cambridge, the Vienna Drosophila Resource Center, James Kennison, Toshiro Aigaki, Beth Stronach, Hugo Bellen, Cahir O'Kane, Stephen Goodwin Mike O'Connor, and Robin Hiesinger for *Drosophila* lines. We thank Toshiro Aigaki, Hugo Bellen, Akira Nakamura, Mike O'Connor, Richard Baines, Alex Whitworth, Iain Robinson, and Peter Ten Dijke for reagents. Thanks also go to Meg Stark (Technology Facility, University of York, York, England, UK) for assistance with transmission EM and Hongru Zhou for help with primary neuronal cultures.

This work was funded by an Alzheimer's Society UK studentship to R.J.H. West, a Biotechnology and Biological Sciences Research Council UK project grant to S.T. Sweeney (BB/I012273/1), National Institutes of Health grants (R01 NS057553 and RO1 NS066586) to F.-B. Gao, and National Institute of Neurological Disorders and Stroke grant (SC2NS077924) to B. Marie.

The authors declare no competing financial interests.

Submitted: 11 April 2014
Accepted: 3 February 2015

References

Aberle, H., A.P. Haghighi, R.D. Fetter, B.D. McCabe, T.R. Magalhães, and C.S. Goodman. 2002. wishful thinking encodes a BMP type II receptor that regulates synaptic growth in *Drosophila*. *Neuron*. 33:545–558. http://dx.doi.org/10.1016/S0896-6273(02)00589-5

Ahmad, S.T., S.T. Sweeney, J.-A. Lee, N.T. Sweeney, and F.-B. Gao. 2009. Genetic screen identifies serpin5 as a regulator of the toll pathway and CHMP2B toxicity associated with frontotemporal dementia. *Proc. Natl. Acad. Sci. USA*. 106:12168–12173. http://dx.doi.org/10.1073/pnas.0903134106

Ang, A.L., H. Fölsch, U.M. Koivisto, M. Pypaert, and I. Mellman. 2003. The Rab8 GTPase selectively regulates AP-1B–dependent basolateral transport in polarized Madin-Darby canine kidney cells. *J. Cell Biol.* 163:339–350. http://dx.doi.org/10.1083/jcb.200307046

Antoniou, X., and T. Borsello. 2012. The JNK signalling transduction pathway in the brain. *Front Biosci (Elite Ed)*. E4:2110–2120. http://dx.doi.org/10.2741/E528

Baines, R.A. 2004. Synaptic strengthening mediated by bone morphogenetic protein-dependent retrograde signaling in the *Drosophila* CNS. *J. Neurosci.* 24:6904–6911. http://dx.doi.org/10.1523/JNEUROSCI.1978-04.2004

Baker, M., I.R. Mackenzie, S.M. Pickering-Brown, J. Gass, R. Rademakers, C. Lindholm, J. Snowden, J. Adamson, A.D. Sadovnick, S. Rollinson, et al. 2006. Mutations in progranulin cause tau-negative frontotemporal dementia linked to chromosome 17. *Nature*. 442:916–919. http://dx.doi.org/10.1038/nature05016

Berke, B., J. Wittnam, E. McNeill, D.L. Van Vactor, and H. Keshishian. 2013. Retrograde BMP signaling at the synapse: a permissive signal for synapse maturation and activity-dependent plasticity. *J. Neurosci.* 33:17937–17950. http://dx.doi.org/10.1523/JNEUROSCI.6075-11.2013

Borroni, B., C. Bonvicini, A. Alberici, E. Buratti, C. Agosti, S. Archetti, A. Papetti, C. Stuani, M. Di Luca, M. Gennarelli, and A. Padovani. 2009. Mutation within TARDBP leads to frontotemporal dementia without motor neuron disease. *Hum. Mutat.* 30:E974–E983. http://dx.doi.org/10.1002/humu.21100

Brown, T.C., S.S. Correia, C.N. Petrok, and J.A. Esteban. 2007. Functional compartmentalization of endosomal trafficking for the synaptic delivery of AMPA receptors during long-term potentiation. *J. Neurosci.* 27:13311–13315. http://dx.doi.org/10.1523/JNEUROSCI.4258-07.2007

Chan, C.-C., S. Scoggin, D. Wang, S. Cherry, T. Dembo, B. Greenberg, E.J. Jin, C. Kuey, A. Lopez, S.Q. Mehta, et al. 2011. Systematic discovery of Rab GTPases with synaptic functions in *Drosophila*. *Curr. Biol.* 21:1704–1715. http://dx.doi.org/10.1016/j.cub.2011.08.058

Collins, C.A., Y.P. Wairkar, S.L. Johnson, and A. DiAntonio. 2006. Highwire restrains synaptic growth by attenuating a MAP kinase signal. *Neuron*. 51:57–69. http://dx.doi.org/10.1016/j.neuron.2006.05.026

Cox, L.E., L. Ferraiuolo, E.F. Goodall, P.R. Heath, A. Higginbottom, H. Mortiboys, H.C. Hollinger, J.A. Hartley, A. Brockington, C.E. Burness, et al. 2010. Mutations in CHMP2B in lower motor neuron predominant amyotrophic lateral sclerosis (ALS). *PLoS ONE*. 5:e9872. http://dx.doi.org/10.1371/journal.pone.0009872

Cruts, M., I. Gijselinck, J. van der Zee, S. Engelborghs, H. Wils, D. Pirici, R. Rademakers, R. Vandenberghe, B. Dermaut, J.-J. Martin, et al. 2006. Null mutations in progranulin cause ubiquitin-positive frontotemporal dementia linked to chromosome 17q21. *Nature*. 442:920–924. http://dx.doi.org/10.1038/nature05017

Davis, G.W., C.M. Schuster, and C.S. Goodman. 1997. Genetic analysis of the mechanisms controlling target selection: target-derived Fasciclin II regulates the pattern of synapse formation. *Neuron*. 19:561–573. http://dx.doi.org/10.1016/S0896-6273(00)80372-4

DeJesus-Hernandez, M., I.R. Mackenzie, B.F. Boeve, A.L. Boxer, M. Baker, N.J. Rutherford, A.M. Nicholson, N.A. Finch, H. Flynn, J. Adamson, et al. 2011. Expanded GGGGCC hexanucleotide repeat in noncoding region of C9ORF72 causes chromosome 9p-linked FTD and ALS. *Neuron*. 72:245–256. http://dx.doi.org/10.1016/j.neuron.2011.09.011

Delaney, J.R., S. Stöven, H. Uvell, K.V. Anderson, Y. Engström, and M. Mlodzik. 2006. Cooperative control of *Drosophila* immune responses by the JNK and NF-kappaB signaling pathways. *EMBO J.* 25:3068–3077. http://dx.doi.org/10.1038/sj.emboj.7601182

Derynck, R., and Y.E. Zhang. 2003. Smad-dependent and Smad-independent pathways in TGF-β family signalling. *Nature*. 425:577–584. http://dx.doi.org/10.1038/nature02006

Engel, M.E., M.A. McDonnell, B.K. Law, and H.L. Moses. 1999. Interdependent SMAD and JNK signaling in transforming growth factor-β-mediated transcription. *J. Biol. Chem.* 274:37413–37420. http://dx.doi.org/10.1074/jbc.274.52.37413

Eresh, S., J. Riese, D.B. Jackson, D. Bohmann, and M. Bienz. 1997. A CREB-binding site as a target for decapentaplegic signalling during *Drosophila* endoderm induction. *EMBO J.* 16:2014–2022. http://dx.doi.org/10.1093/emboj/16.8.2014

Esseltine, J.L., F.M. Ribeiro, and S.S.G. Ferguson. 2012. Rab8 modulates metabotropic glutamate receptor subtype 1 intracellular trafficking and signaling in a protein kinase C-dependent manner. *J. Neurosci.* 32:16933–16942. http://dx.doi.org/10.1523/JNEUROSCI.0625-12.2012

Filimonenko, M., S. Stuffers, C. Raiborg, A. Yamamoto, L. Malerød, E.M.C. Fisher, A. Isaacs, A. Brech, H. Stenmark, and A. Simonsen. 2007. Functional multivesicular bodies are required for autophagic clearance of protein aggregates associated with neurodegenerative disease. *J. Cell Biol.* 179:485–500. http://dx.doi.org/10.1083/jcb.200702115

Freeman, M. 1996. Reiterative use of the EGF receptor triggers differentiation of all cell types in the *Drosophila* eye. *Cell*. 87:651–660. http://dx.doi.org/10.1016/S0092-8674(00)81385-9

Fuentes-Medel, Y., J. Ashley, R. Barria, R. Maloney, M. Freeman, and V. Budnik. 2012. Integration of a retrograde signal during synapse formation by glia-secreted TGF-β ligand. *Curr. Biol.* 22:1831–1838. http://dx.doi.org/10.1016/j.cub.2012.07.063

Fukuda, T., L. Ewan, M. Bauer, R.J. Mattaliano, K. Zaal, E. Ralston, P.H. Plotz, and N. Raben. 2006. Dysfunction of endocytic and autophagic pathways in a lysosomal storage disease. *Ann. Neurol.* 59:700–708. http://dx.doi.org/10.1002/ana.20807

Gascon, E., K. Lynch, H. Ruan, S. Almeida, J.M. Verheyden, W.W. Seeley, D.W. Dickson, L. Petrucelli, D. Sun, J. Jiao, et al. 2014. Alterations in microRNA-124 and AMPA receptors contribute to social behavioral deficits in frontotemporal dementia. *Nat. Med.* 20:1444–1451. http://dx.doi.org/10.1038/nm.3717

Gerges, N.Z., D.S. Backos, and J.A. Esteban. 2004. Local control of AMPA receptor trafficking at the postsynaptic terminal by a small GTPase of the Rab family. *J. Biol. Chem.* 279:43870–43878. http://dx.doi.org/10.1074/jbc.M404982200

Giagtzoglou, N., S. Yamamoto, D. Zitserman, H.K. Graves, K.L. Schulze, H. Wang, H. Klein, F. Roegiers, and H.J. Bellen. 2012. *dEHBP1* controls exocytosis and recycling of Delta during asymmetric divisions. *J. Cell Biol.* 196:65–83. http://dx.doi.org/10.1083/jcb.201106088

Goold, C.P., and G.W. Davis. 2007. The BMP ligand Gbb gates the expression of synaptic homeostasis independent of synaptic growth control. *Neuron*. 56:109–123. http://dx.doi.org/10.1016/j.neuron.2007.08.006

Hardy, J., and E. Rogaeva. 2013. Motor neuron disease and frontotemporal dementia: sometimes related, sometimes not. *Exp. Neurol.* 262(Pt. B):75–83.

Henne, W.M., N.J. Buchkovich, and S.D. Emr. 2011. The ESCRT pathway. *Dev. Cell*. 21:77–91. http://dx.doi.org/10.1016/j.devcel.2011.05.015

Huber, L.A., M.J. de Hoop, P. Dupree, M. Zerial, K. Simons, and C. Dotti. 1993a. Protein transport to the dendritic plasma membrane of cultured neurons is regulated by rab8p. *J. Cell Biol.* 123:47–55. http://dx.doi.org/10.1083/jcb.123.1.47

Huber, L.A., S. Pimplikar, R.G. Parton, H. Virta, M. Zerial, and K. Simons. 1993b. Rab8, a small GTPase involved in vesicular traffic between the TGN and the basolateral plasma membrane. *J. Cell Biol.* 123:35–45. http://dx.doi.org/10.1083/jcb.123.1.35

Hutton, M., C.L. Lendon, P. Rizzu, M. Baker, S. Froelich, H. Houlden, S. Pickering-Brown, S. Chakraverty, A. Isaacs, A. Grover, et al. 1998. Association of missense and 5′-splice-site mutations in tau with the inherited dementia FTDP-17. *Nature*. 393:702–705. http://dx.doi.org/10.1038/31508

Inoue, H., T. Imamura, Y. Ishidou, M. Takase, Y. Udagawa, Y. Oka, K. Tsuneizumi, T. Tabata, K. Miyazono, and M. Kawabata. 1998. Interplay of signal mediators of decapentaplegic (Dpp): molecular characterization of mothers against dpp, Medea, and daughters against dpp. *Mol. Biol. Cell*. 9:2145–2156. http://dx.doi.org/10.1091/mbc.9.8.2145

Jékely, G., and P. Rørth. 2003. Hrs mediates downregulation of multiple signalling receptors in *Drosophila*. *EMBO Rep.* 4:1163–1168. http://dx.doi.org/10.1038/sj.embor.7400019

Kasprowicz, J., S. Kuenen, K. Miskiewicz, R.L.P. Habets, L. Smitz, and P. Verstreken. 2008. Inactivation of clathrin heavy chain inhibits synaptic recycling but allows bulk membrane uptake. *J. Cell Biol.* 182:1007–1016.

Kawasaki, F., J. Iyer, L.L. Posey, C.E. Sun, S.E. Mammen, H. Yan, and R.W. Ordway. 2011. The DISABLED protein functions in CLATHRIN-mediated synaptic vesicle endocytosis and exoendocytic coupling at the active zone. *Proc. Natl. Acad. Sci. USA*. 108:E222–E229. http://dx.doi.org/10.1073/pnas.1102231108

Kim, G.-H., E. Park, Y.-Y. Kong, and J.-K. Han. 2006. Novel function of POSH, a JNK scaffold, as an E3 ubiquitin ligase for the Hrs stability on early endosomes. *Cell. Signal.* 18:553–563. http://dx.doi.org/10.1016/j.cellsig.2005.05.026

Kovacs, G.G., J.R. Murrell, S. Horvath, L. Haraszti, K. Majtenyi, M.J. Molnar, H. Budka, B. Ghetti, and S. Spina. 2009. TARDBP variation associated with frontotemporal dementia, supranuclear gaze palsy, and chorea. *Mov. Disord.* 24:1843–1847.

Kukekov, N.V., Z. Xu, and L.A. Greene. 2006. Direct interaction of the molecular scaffolds POSH and JIP is required for apoptotic activation of JNKs. *J. Biol. Chem.* 281:15517–15524. http://dx.doi.org/10.1074/jbc.M601056200

Lee, J.-A., A. Beigneux, S.T. Ahmad, S.G. Young, and F.-B. Gao. 2007. ESCRT-III dysfunction causes autophagosome accumulation and neurodegeneration. *Curr. Biol.* 17:1561–1567. http://dx.doi.org/10.1016/j.cub.2007.07.029

Lee, Y.S., and R.W. Carthew. 2003. Making a better RNAi vector for *Drosophila*: use of intron spacers. *Methods*. 30:322–329. http://dx.doi.org/10.1016/S1046-2023(03)00051-3

Lennox, A.L., and B. Stronach. 2010. POSH misexpression induces caspase-dependent cell death in *Drosophila*. *Dev. Dyn.* 239:651–664. http://dx.doi.org/10.1002/dvdy.22186

Ling, S.-C., M. Polymenidou, and D.W. Cleveland. 2013. Converging mechanisms in ALS and FTD: disrupted RNA and protein homeostasis. *Neuron*. 79:416–438. http://dx.doi.org/10.1016/j.neuron.2013.07.033

Lloyd, T.E., R. Atkinson, M.N. Wu, Y. Zhou, G. Pennetta, and H.J. Bellen. 2002. Hrs regulates endosome membrane invagination and tyrosine kinase receptor signaling in *Drosophila*. *Cell*. 108:261–269. http://dx.doi.org/10.1016/S0092-8674(02)00611-6

Lu, Y., Z. Zhang, D. Sun, S.T. Sweeney, and F.-B. Gao. 2013. Syntaxin 13, a genetic modifier of mutant CHMP2B in frontotemporal dementia, is required for autophagosome maturation. *Mol. Cell*. 52:264–271. http://dx.doi.org/10.1016/j.molcel.2013.08.041

Maldonado, C., D. Alicea, M. Gonzalez, M. Bykhovskaia, and B. Marie. 2013. Adar is essential for optimal presynaptic function. *Mol. Cell. Neurosci.* 52:173–180. http://dx.doi.org/10.1016/j.mcn.2012.10.009

Mao, R., Y. Fan, Y. Mou, H. Zhang, S. Fu, and J. Yang. 2011. TAK1 lysine 158 is required for TGF-β-induced TRAF6-mediated Smad-independent IKK/NF-κB and JNK/AP-1 activation. *Cell. Signal.* 23:222–227. http://dx.doi.org/10.1016/j.cellsig.2010.09.006

Marie, B., S.T. Sweeney, K.E. Poskanzer, J. Roos, R.B. Kelly, and G.W. Davis. 2004. Dap160/intersectin scaffolds the periactive zone to achieve high-fidelity endocytosis and normal synaptic growth. *Neuron*. 43:207–219. http://dx.doi.org/10.1016/j.neuron.2004.07.001

Marqués, G. 2005. Morphogens and synaptogenesis in *Drosophila*. *J. Neurobiol.* 64:417–434. http://dx.doi.org/10.1002/neu.20165

Marqués, G., H. Bao, T.E. Haerry, M.J. Shimell, P. Duchek, B. Zhang, and M.B. O'Connor. 2002. The *Drosophila* BMP type II receptor Wishful Thinking regulates neuromuscular synapse morphology and function. *Neuron*. 33:529–543. http://dx.doi.org/10.1016/S0896-6273(02)00595-0

Martín-Blanco, E., A. Gampel, J. Ring, K. Virdee, N. Kirov, A.M. Tolkovsky, and A. Martinez-Arias. 1998. puckered encodes a phosphatase that mediates a feedback loop regulating JNK activity during dorsal closure in *Drosophila*. *Genes Dev.* 12:557–570. http://dx.doi.org/10.1101/gad.12.4.557

Massagué, J. 2012. TGFβ signalling in context. *Nat. Rev. Mol. Cell Biol.* 13:616–630. http://dx.doi.org/10.1038/nrm3434

McCabe, B.D., G. Marqués, A.P. Haghighi, R.D. Fetter, M.L. Crotty, T.E. Haerry, C.S. Goodman, and M.B. O'Connor. 2003. The BMP homolog Gbb provides a retrograde signal that regulates synaptic growth at the *Drosophila* neuromuscular junction. *Neuron*. 39:241–254. http://dx.doi.org/10.1016/S0896-6273(03)00426-4

McCabe, B.D., S. Hom, H. Aberle, R.D. Fetter, G. Marqués, T.E. Haerry, H. Wan, M.B. O'Connor, C.S. Goodman, and A.P. Haghighi. 2004. Highwire regulates presynaptic BMP signaling essential for synaptic growth. *Neuron*. 41:891–905. http://dx.doi.org/10.1016/S0896-6273(04)00073-X

Mihaly, J., L. Kockel, K. Gaengel, U. Weber, D. Bohmann, and M. Mlodzik. 2001. The role of the *Drosophila* TAK homologue dTAK during development. *Mech. Dev.* 102:67–79. http://dx.doi.org/10.1016/S0925-4773(01)00285-4

Milton, V.J., H.E. Jarrett, K. Gowers, S. Chalak, L. Briggs, I.M. Robinson, and S.T. Sweeney. 2011. Oxidative stress induces overgrowth of the *Drosophila* neuromuscular junction. *Proc. Natl. Acad. Sci. USA*. 108:17521–17526. http://dx.doi.org/10.1073/pnas.1014511108

Moritz, O.L., B.M. Tam, L.L. Hurd, J. Peränen, D. Deretic, and D.S. Papermaster. 2001. Mutant rab8 Impairs docking and fusion of rhodopsin-bearing post-Golgi membranes and causes cell death of transgenic *Xenopus* rods. *Mol. Biol. Cell*. 12:2341–2351. http://dx.doi.org/10.1091/mbc.12.8.2341

Neubert, M., D.A. Ridder, P. Bargiotas, S. Akira, and M. Schwaninger. 2011. Acute inhibition of TAK1 protects against neuronal death in cerebral ischemia. *Cell Death Differ.* 18:1521–1530. http://dx.doi.org/10.1038/cdd.2011.29

O'Connor-Giles, K.M., L.L. Ho, and B. Ganetzky. 2008. Nervous wreck interacts with thickveins and the endocytic machinery to attenuate retrograde BMP signaling during synaptic growth. *Neuron*. 58:507–518. http://dx.doi.org/10.1016/j.neuron.2008.03.007

Parkinson, N., P.G. Ince, M.O. Smith, R. Highley, G. Skibinski, P.M. Andersen, K.E. Morrison, H.S. Pall, O. Hardiman, J. Collinge, et al. FReJA Consortium. 2006. ALS phenotypes with mutations in CHMP2B (charged multivesicular body protein 2B). *Neurology*. 67:1074–1077. http://dx.doi.org/10.1212/01.wnl.0000231510.89311.8b

Pauli, A., F. Althoff, R.A. Oliveira, S. Heidmann, O. Schuldiner, C.F. Lehner, B.J. Dickson, and K. Nasmyth. 2008. Cell-type-specific TEV protease cleavage reveals cohesin functions in *Drosophila* neurons. *Dev. Cell*. 14:239–251. http://dx.doi.org/10.1016/j.devcel.2007.12.009

Perlman, R., W.P. Schiemann, M.W. Brooks, H.F. Lodish, and R.A. Weinberg. 2001. TGF-β-induced apoptosis is mediated by the adapter protein Daxx that facilitates JNK activation. *Nat. Cell Biol.* 3:708–714. http://dx.doi.org/10.1038/35087019

Persson, U., H. Izumi, S. Souchelnytskyi, S. Itoh, S. Grimsby, U. Engström, C.H. Heldin, K. Funa, and P. ten Dijke. 1998. The L45 loop in type I receptors for TGF-β family members is a critical determinant in specifying Smad isoform activation. *FEBS Lett.* 434:83–87. http://dx.doi.org/10.1016/S0014-5793(98)00954-5

Pulipparacharuvil, S., M.A. Akbar, S. Ray, E.A. Sevrioukov, A.S. Haberman, J. Rohrer, and H. Krämer. 2005. *Drosophila* Vps16A is required for trafficking to lysosomes and biogenesis of pigment granules. *J. Cell Sci.* 118:3663–3673. http://dx.doi.org/10.1242/jcs.02502

Rawson, J.M., M. Lee, E.L. Kennedy, and S.B. Selleck. 2003. *Drosophila* neuromuscular synapse assembly and function require the TGF-β type I receptor saxophone and the transcription factor Mad. *J. Neurobiol.* 55:134–150. http://dx.doi.org/10.1002/neu.10189

Renton, A.E., E. Majounie, A. Waite, J. Simón-Sánchez, S. Rollinson, J.R. Gibbs, J.C. Schymick, H. Laaksovirta, J.C. van Swieten, L. Myllykangas, et al. ITALSGEN Consortium. 2011. A hexanucleotide repeat expansion in C9ORF72 is the cause of chromosome 9p21-linked ALS-FTD. *Neuron*. 72:257–268. http://dx.doi.org/10.1016/j.neuron.2011.09.010

Ringholz, G.M., and S.R. Greene. 2006. The relationship between amyotrophic lateral sclerosis and frontotemporal dementia. *Curr. Neurol. Neurosci. Rep.* 6:387–392. http://dx.doi.org/10.1007/s11910-996-0019-6

Robinson, I.M., R. Ranjan, and T.L. Schwarz. 2002. Synaptotagmins I and IV promote transmitter release independently of Ca(2+) binding in the C(2)A domain. *Nature*. 418:336–340. http://dx.doi.org/10.1038/nature00915

Rodal, A.A., A.D. Blunk, Y. Akbergenova, R.A. Jorquera, L.K. Buhl, and J.T. Littleton. 2011. A presynaptic endosomal trafficking pathway controls synaptic growth signaling. *J. Cell Biol.* 193:201–217. http://dx.doi.org/10.1083/jcb.201009052

Rusten, T.E., T. Vaccari, K. Lindmo, L.M.W. Rodahl, I.P. Nezis, C. Sem-Jacobsen, F. Wendler, J.-P. Vincent, A. Brech, D. Bilder, and H. Stenmark. 2007. ESCRTs and Fab1 regulate distinct steps of autophagy. *Curr. Biol.* 17:1817–1825. http://dx.doi.org/10.1016/j.cub.2007.09.032

Ryder, E., M. Ashburner, R. Bautista-Llacer, J. Drummond, J. Webster, G. Johnson, T. Morley, Y.S. Chan, F. Blows, D. Coulson, et al. 2007. The DrosDel deletion collection: a *Drosophila* genomewide chromosomal deficiency resource. *Genetics*. 177:615–629. http://dx.doi.org/10.1534/genetics.107.076216

Sanyal, S. 2009. Genomic mapping and expression patterns of C380, OK6 and D42 enhancer trap lines in the larval nervous system of *Drosophila*. *Gene Expr. Patterns*. 9:371–380. http://dx.doi.org/10.1016/j.gep.2009.01.002

Sanyal, S., D.J. Sandstrom, C.A. Hoeffer, and M. Ramaswami. 2002. AP-1 functions upstream of CREB to control synaptic plasticity in *Drosophila*. *Nature*. 416:870–874. http://dx.doi.org/10.1038/416870a

Sato, T., S. Mushiake, Y. Kato, K. Sato, M. Sato, N. Takeda, K. Ozono, K. Miki, Y. Kubo, A. Tsuji, et al. 2007. The Rab8 GTPase regulates apical protein localization in intestinal cells. *Nature*. 448:366–369. http://dx.doi.org/10.1038/nature05929

Sato, T., T. Iwano, M. Kunii, S. Matsuda, R. Mizuguchi, Y. Jung, H. Hagiwara, Y. Yoshihara, M. Yuzaki, R. Harada, and A. Harada. 2014. Rab8a and Rab8b are essential for several apical transport pathways but insufficient for ciliogenesis. *J. Cell Sci.* 127:422–431. http://dx.doi.org/10.1242/jcs.136903

Sekelsky, J.J., S.J. Newfeld, L.A. Raftery, E.H. Chartoff, and W.M. Gelbart. 1995. Genetic characterization and cloning of mothers against dpp, a gene required for decapentaplegic function in *Drosophila melanogaster*. *Genetics*. 139:1347–1358.

Seto, E.S., H.J. Bellen, and T.E. Lloyd. 2002. When cell biology meets development: endocytic regulation of signaling pathways. *Genes Dev.* 16:1314–1336. http://dx.doi.org/10.1101/gad.989602

Shi, W., Y. Chen, G. Gan, D. Wang, J. Ren, Q. Wang, Z. Xu, W. Xie, and Y.Q. Zhang. 2013. Brain tumor regulates neuromuscular synapse growth and endocytosis in *Drosophila* by suppressing mad expression. *J. Neurosci.* 33:12352–12363. http://dx.doi.org/10.1523/JNEUROSCI.0386-13.2013

Shimizu, H., S. Kawamura, and K. Ozaki. 2003. An essential role of Rab5 in uniformity of synaptic vesicle size. *J. Cell Sci.* 116:3583–3590. http://dx.doi.org/10.1242/jcs.00676

Skibinski, G., N.J. Parkinson, J.M. Brown, L. Chakrabarti, S.L. Lloyd, H. Hummerich, J.E. Nielsen, J.R. Hodges, M.G. Spillantini, T. Thusgaard, et al. 2005. Mutations in the endosomal ESCRTIII-complex subunit CHMP2B in frontotemporal dementia. *Nat. Genet.* 37:806–808. http://dx.doi.org/10.1038/ng1609

Smith, R.B., J.B. Machamer, N.C. Kim, T.S. Hays, and G. Marqués. 2012. Relay of retrograde synaptogenic signals through axonal transport of BMP receptors. *J. Cell Sci.* 125:3752–3764. http://dx.doi.org/10.1242/jcs.094292

Sorrentino, A., N. Thakur, S. Grimsby, A. Marcusson, V. von Bulow, N. Schuster, S. Zhang, C.-H. Heldin, and M. Landström. 2008. The type I TGF-β receptor engages TRAF6 to activate TAK1 in a receptor kinase-independent manner. *Nat. Cell Biol.* 10:1199–1207. http://dx.doi.org/10.1038/ncb1780

Sweeney, N.T., J.E. Brenman, Y.N. Jan, and F.B. Gao. 2006. The coiled-coil protein shrub controls neuronal morphogenesis in *Drosophila*. *Curr. Biol.* 16:1006–1011. http://dx.doi.org/10.1016/j.cub.2006.03.067

Sweeney, S.T., and G.W. Davis. 2002. Unrestricted synaptic growth in spinster-a late endosomal protein implicated in TGF-β-mediated synaptic growth regulation. *Neuron*. 36:403–416. http://dx.doi.org/10.1016/S0896-6273(02)01014-0

Tanaka, T., and A. Nakamura. 2008. The endocytic pathway acts downstream of Oskar in *Drosophila* germ plasm assembly. *Development*. 135:1107–1117. http://dx.doi.org/10.1242/dev.017293

Tapon, N., K. Nagata, N. Lamarche, and A. Hall. 1998. A new rac target POSH is an SH3-containing scaffold protein involved in the JNK and NF-kappaB signalling pathways. *EMBO J.* 17:1395–1404. http://dx.doi.org/10.1093/emboj/17.5.1395

Tsuda, M., C. Langmann, N. Harden, and T. Aigaki. 2005. The RING-finger scaffold protein Plenty of SH3s targets TAK1 to control immunity signalling in *Drosophila*. *EMBO Rep.* 6:1082–1087. http://dx.doi.org/10.1038/sj.embor.7400537

Tsuda, M., K.-H. Seong, and T. Aigaki. 2006. POSH, a scaffold protein for JNK signaling, binds to ALG-2 and ALIX in *Drosophila*. *FEBS Lett.* 580:3296–3300. http://dx.doi.org/10.1016/j.febslet.2006.05.005

Tsuneizumi, K., T. Nakayama, Y. Kamoshida, T.B. Kornberg, J.L. Christian, and T. Tabata. 1997. Daughters against dpp modulates dpp organizing activity in *Drosophila* wing development. *Nature*. 389:627–631. http://dx.doi.org/10.1038/39362

Urwin, H., A. Authier, J.E. Nielsen, D. Metcalf, C. Powell, K. Froud, D.S. Malcolm, I. Holm, P. Johannsen, J. Brown, et al. FReJA Consortium. 2010. Disruption of endocytic trafficking in frontotemporal dementia with CHMP2B mutations. *Hum. Mol. Genet.* 19:2228–2238. http://dx.doi.org/10.1093/hmg/ddq100

van Blitterswijk, M., L. Vlam, M.A. van Es, W.L. van der Pol, E.A. Hennekam, D. Dooijes, H.J. Schelhaas, A.J. van der Kooi, M. de Visser, J.H. Veldink,

and L.H. van den Berg. 2012. Genetic overlap between apparently sporadic motor neuron diseases. *PLoS ONE*. 7:e48983. http://dx.doi.org/10.1371/journal.pone.0048983

Van Langenhove, T., J. van der Zee, and C. Van Broeckhoven. 2012. The molecular basis of the frontotemporal lobar degeneration-amyotrophic lateral sclerosis spectrum. *Ann. Med.* 44:817–828. http://dx.doi.org/10.3109/07853890.2012.665471

Vanlandingham, P.A., T.R. Fore, L.R. Chastain, S.M. Royer, H. Bao, N.E. Reist, and B. Zhang. 2013. Epsin 1 promotes synaptic growth by enhancing BMP signal levels in motoneuron nuclei. *PLoS ONE*. 8:e65997. http://dx.doi.org/10.1371/journal.pone.0065997

Votteler, J., E. Iavnilovitch, O. Fingrut, V. Shemesh, D. Taglicht, O. Erez, S. Sörgel, T. Walther, N. Bannert, U. Schubert, and Y. Reiss. 2009. Exploring the functional interaction between POSH and ALIX and the relevance to HIV-1 release. *BMC Biochem.* 10:12. http://dx.doi.org/10.1186/1471-2091-10-12

Wan, H.I., A. DiAntonio, R.D. Fetter, K. Bergstrom, R. Strauss, and C.S. Goodman. 2000. Highwire regulates synaptic growth in *Drosophila*. *Neuron*. 26:313–329. http://dx.doi.org/10.1016/S0896-6273(00)81166-6

Wang, X., W.R. Shaw, H.T.H. Tsang, E. Reid, and C.J. O'Kane. 2007. *Drosophila* spichthyin inhibits BMP signaling and regulates synaptic growth and axonal microtubules. *Nat. Neurosci.* 10:177–185. http://dx.doi.org/10.1038/nn1841

Watts, G.D.J., J. Wymer, M.J. Kovach, S.G. Mehta, S. Mumm, D. Darvish, A. Pestronk, M.P. Whyte, and V.E. Kimonis. 2004. Inclusion body myopathy associated with Paget disease of bone and frontotemporal dementia is caused by mutant valosin-containing protein. *Nat. Genet.* 36:377–381. http://dx.doi.org/10.1038/ng1332

Wheaton, M.W., A.R. Salamone, D.M. Mosnik, R.O. McDonald, S.H. Appel, H.I. Schmolck, G.M. Ringholz, and P.E. Schulz. 2007. Cognitive impairment in familial ALS. *Neurology*. 69:1411–1417. http://dx.doi.org/10.1212/01.wnl.0000277422.11236.2c

Winther, A.M.E., W. Jiao, O. Vorontsova, K.A. Rees, T.W. Koh, E. Sopova, K.L. Schulze, H.J. Bellen, and O. Shupliakov. 2013. The dynamin-binding domains of Dap160/intersectin affect bulk membrane retrieval in synapses. *J. Cell Sci.* 126:1021–1031. http://dx.doi.org/10.1242/jcs.118968

Xiao, L., N. Michalski, E. Kronander, E. Gjoni, C. Genoud, G. Knott, and R. Schneggenburger. 2013. BMP signaling specifies the development of a large and fast CNS synapse. *Nat. Neurosci.* 16:856–864. http://dx.doi.org/10.1038/nn.3414

Xu, Z., N.V. Kukekov, and L.A. Greene. 2003. POSH acts as a scaffold for a multiprotein complex that mediates JNK activation in apoptosis. *EMBO J.* 22:252–261. http://dx.doi.org/10.1093/emboj/cdg021

Xu, Z., N.V. Kukekov, and L.A. Greene. 2005. Regulation of apoptotic c-Jun N-terminal kinase signaling by a stabilization-based feed-forward loop. *Mol. Cell. Biol.* 25:9949–9959. http://dx.doi.org/10.1128/MCB.25.22.9949-9959.2005

Yamaguchi, K., K. Shirakabe, H. Shibuya, K. Irie, I. Oishi, N. Ueno, T. Taniguchi, E. Nishida, and K. Matsumoto. 1995. Identification of a member of the MAPKKK family as a potential mediator of TGF-beta signal transduction. *Science*. 270:2008–2011. http://dx.doi.org/10.1126/science.270.5244.2008

Zhang, B., Y.H. Koh, R.B. Beckstead, V. Budnik, B. Ganetzky, and H.J. Bellen. 1998. Synaptic vesicle size and number are regulated by a clathrin adaptor protein required for endocytosis. *Neuron.* 21:1465–1475. http://dx.doi.org/10.1016/S0896-6273(00)80664-9

Zhang, J., K.L. Schulze, P.R. Hiesinger, K. Suyama, S. Wang, M. Fish, M. Acar, R.A. Hoskins, H.J. Bellen, and M.P. Scott. 2007. Thirty-one flavors of *Drosophila* rab proteins. *Genetics*. 176:1307–1322. http://dx.doi.org/10.1534/genetics.106.066761

Zhang, Q.-G., R.-M. Wang, X.-H. Yin, J. Pan, T.-L. Xu, and G.-Y. Zhang. 2005. Knock-down of POSH expression is neuroprotective through down-regulating activation of the MLK3-MKK4-JNK pathway following cerebral ischaemia in the rat hippocampal CA1 subfield. *J. Neurochem.* 95:784–795. http://dx.doi.org/10.1111/j.1471-4159.2005.03435.x

Zhang, Q.-G., D. Han, J. Xu, Q. Lv, R. Wang, X.-H. Yin, T.-L. Xu, and G.-Y. Zhang. 2006. Ischemic preconditioning negatively regulates plenty of SH3s-mixed lineage kinase 3-Rac1 complex and c-Jun N-terminal kinase 3 signaling via activation of Akt. *Neuroscience*. 143:431–444. http://dx.doi.org/10.1016/j.neuroscience.2006.07.049

West et al., http://www.jcb.org/cgi/content/full/jcb.201404066/DC1

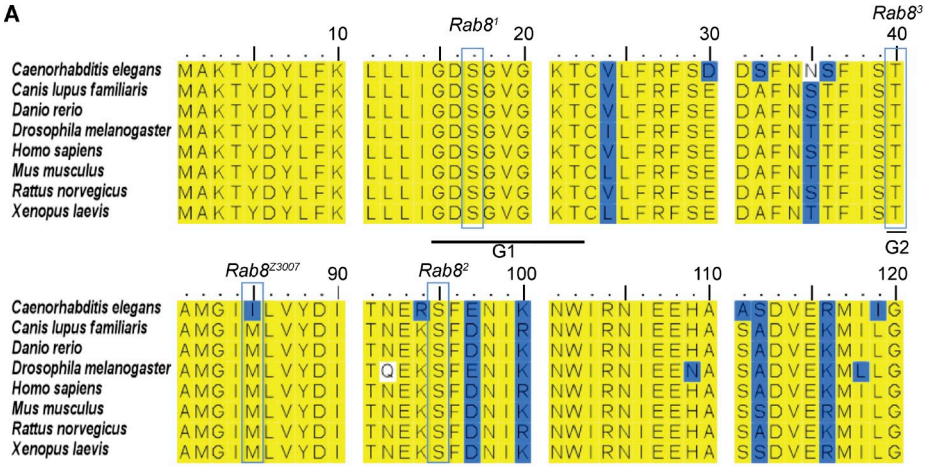

B

	Rab8¹	Rab8²	Rab8³	Rab8Z3007	Rab8B229	Df(3L)ED228
Rab8¹	-	Semi-Lethal	Semi-Lethal	Pharate Lethal	Pharate Lethal	Pharate Lethal
Rab8²	-	-	Pharate Lethal	Pharate Lethal	Pharate Lethal	Pharate Lethal
Rab8³	-	-	-	Pharate Lethal	Pharate Lethal	Pharate Lethal
Rab8Z3007	-	-	-	-	Pharate Lethal	Pharate Lethal
Rab8B229	-	-	-	-	-	Pharate Lethal
Df(3L)ED228	-	-	-	-	-	-

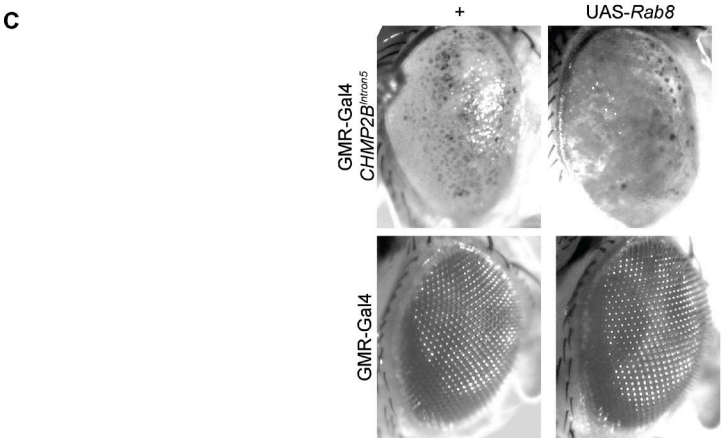

Figure S1. ***Rab8* point mutants affect highly conserved residues within *Rab8* and fail to complement.** (A) Sequence alignment of Rab8 reveals high level of conservation across species. Mapping of *Rab8* mutant alleles to aligned amino acid sequences demonstrates that all *Rab8* mutants affect highly conserved residues. Both $Rab8^{1}$ and $Rab8^{3}$ alter residues within the guanine nucleotide-binding region, composed of five G motifs (G1–G5). G1 and G2 are visible within this section of the alignment. Yellow = 100% conservation; blue = 80% conservation. Accession numbers (NCBI Protein database).: *Caenorhabditis elegans*, BAD07034; *Canis lupus*, CAB56776; *Danio rerio*, AAI34060; *Drosophila*, BAD07038; *Homo sapiens*, AAM21091; *Mus musculus*, NP_075615; *Rattus norvegicus*, AEJ31940; *Xenopus laevis*, NP_001087273. (B) All trans-heterozygous *Rab8* mutant combinations result in lethality, indicating a failure to complement one another. Pharate lethality was not observed in 100% of $Rab8^{1}/Rab8^{2}$ and $Rab8^{1}/Rab8^{3}$ flies; however, those that were not pharate lethal died within ~24 h of eclosion. These were recorded as semilethal. (C) Coexpression of UAS-*Rab8* in the *Drosophila* eye alleviates the severity of the $CHMP2B^{Intron5}$ eye phenotype, resulting in a reduction in the number of melanized puncta seen on the eye. Expression of UAS-*Rab8* under the control of GMR-Gal4 in the absence of $CHMP2B^{Intron5}$ has no affect upon the eye.

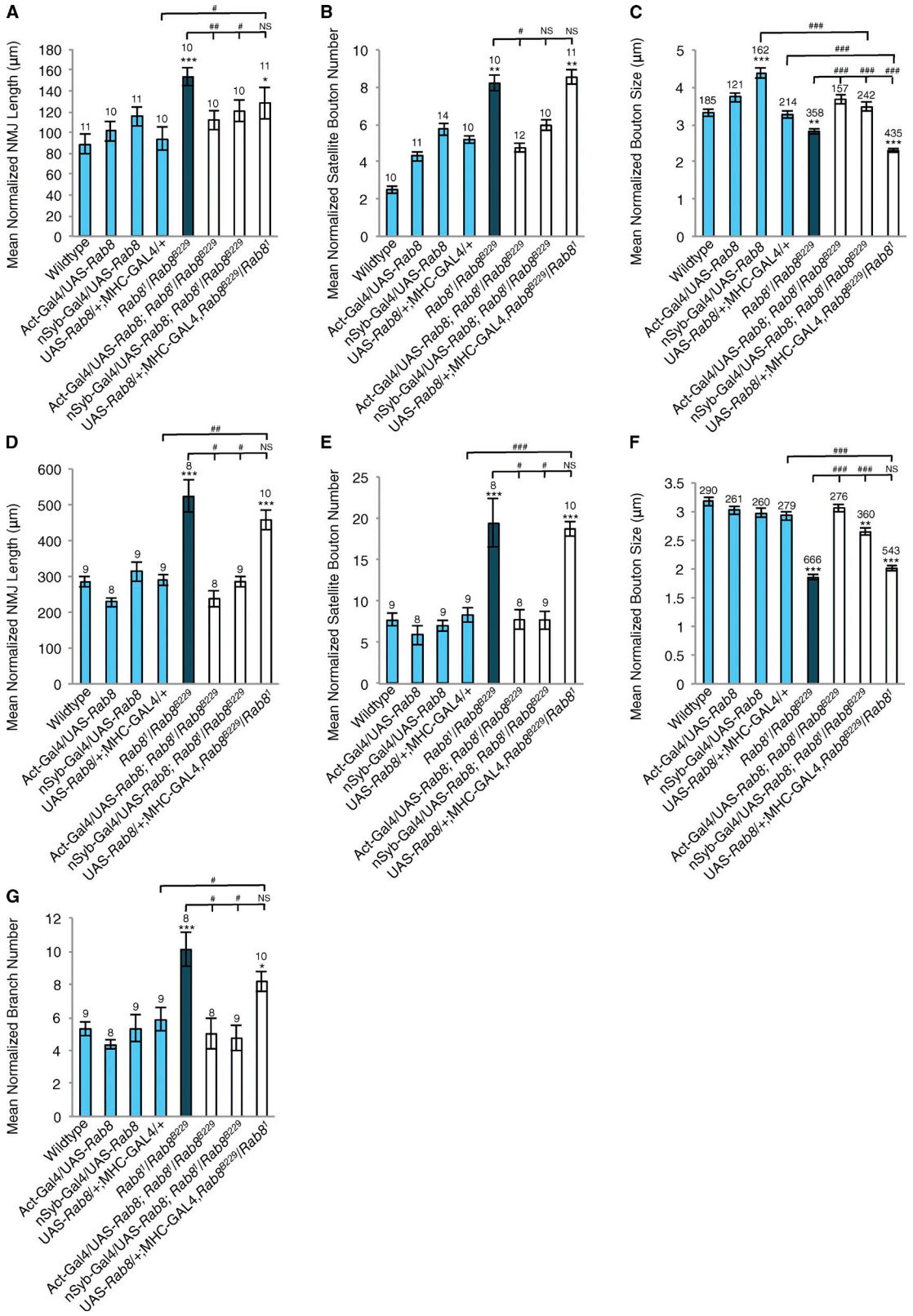

Figure S2. ***Rab8* mutants display unregulated growth at the larval NMJ.** (A–C) *Rab8* mutants display significant unregulated growth at muscle 4 (hemisegment A3, third instar) characterized by increased NMJ length (A), increased satellite bouton number (B), and reduced bouton size (C). All phenotypes are rescued globally (actin-GAL4) and presynaptically (nSyb-GAL4) but not postsynaptically (MHC-GAL4). ANOVA: F(d.f. 7) = 5.2069 (A), 2.6923 (B), and 48.1829 (C); $P < 0.001$ with post-hoc Dunnett's comparison to wild-type controls: ***, $P < 0.001$; **, $P < 0.01$; *, $P < 0.05$. Post-hoc Student's *t* test comparison between groups: ###, $P < 0.001$; ##, $P < 0.01$; #, $P < 0.05$. (D–G) *Rab8* mutants display significant unregulated growth at muscle 6/7 (hemisegment A3, third instar) characterized by increased NMJ length (D), increased satellite bouton number (E), reduced bouton size (F), and increased branch number (G). All phenotypes are rescued globally (actin-GAL4) and presynaptically (nSyb-GAL4) but not postsynaptically (MHC-GAL4). ANOVA: F(d.f. 7) = 18.025 (D), 17.358 (E), 96.347 (C), and 7.189 (G); $P < 0.001$ with post-hoc Dunnett's comparison to wild-type controls: ***, $P < 0.001$; **, $P < 0.01$; *, $P < 0.05$. Post-hoc Student's *t* test comparison between groups: ###, $P < 0.001$; ##, $P < 0.01$; #, $P < 0.05$. Numbers above bars = *n*. Error bars show SEM.

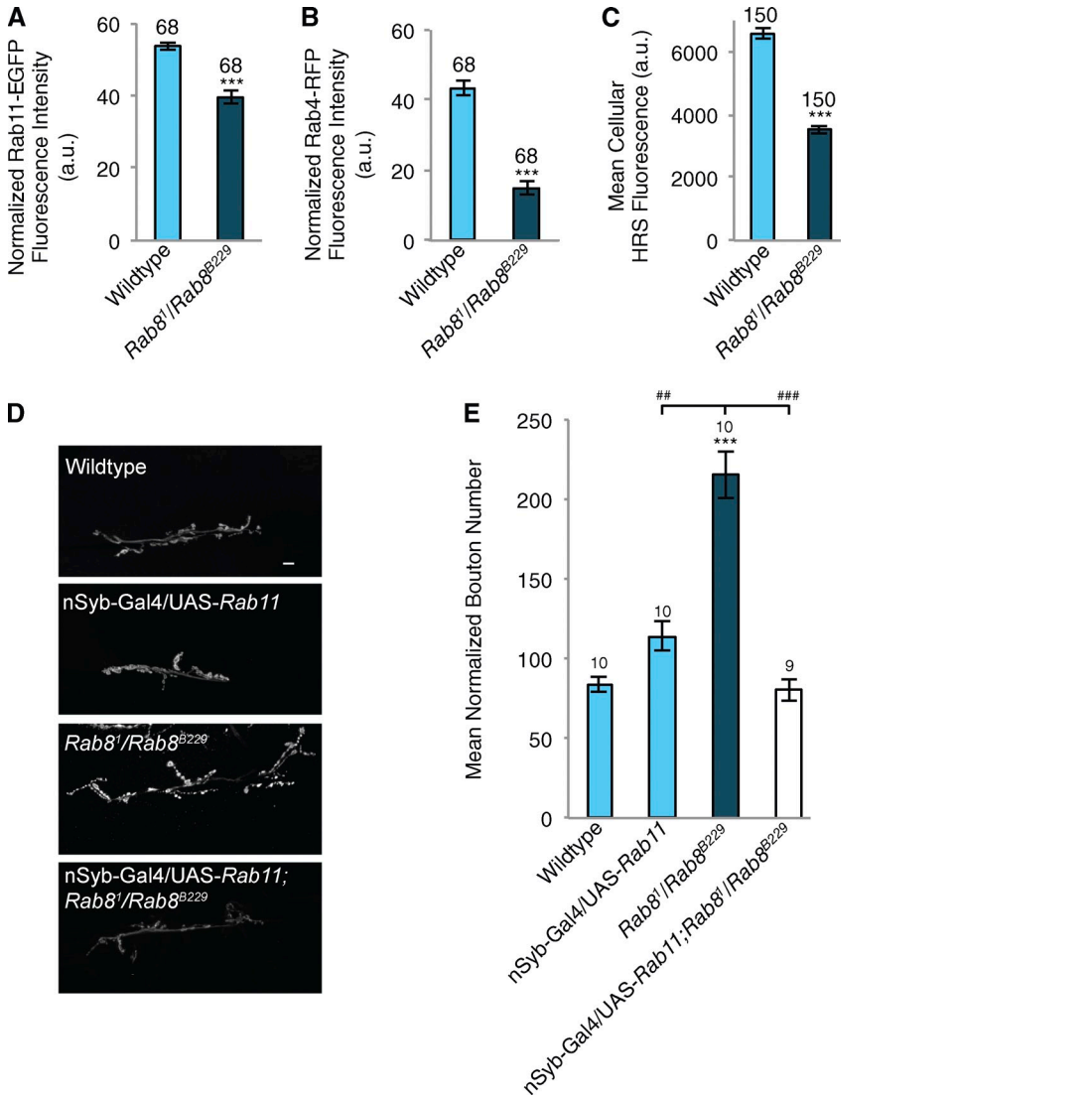

Figure S3. **The recycling endosome is depleted in *Rab8* mutants and Rab11 expression rescues synaptic overgrowth.** (A) Rab11-GFP fluorescence intensity is reduced at synapses in *Rab8* mutants. ANOVA: F(d.f. 1) = 45.078; ***, P < 0.001. (B) Rab4-RFP fluorescence intensity is reduced at synapses in *Rab8* mutants. ANOVA: F(d.f. 1) = 150.422; ***, P < 0.001. (C) Staining intensity for HRS is reduced in motor neuronal cell bodies in *Rab8* mutants. ANOVA: F(d.f. 1) = 215.8528; ***, P < 0.001. a.u., arbitrary unit. (D and E) Panneuronal overexpression of UAS-*Rab11* alleviated synaptic overgrowth in *Rab8* trans-heterozygous mutants (muscle 6/7, hemisegment A3). Bar, 10 µm. ANOVA: F(d.f. 3) = 41.455; P < 0.001 with post-hoc Dunnett's comparison to wild-type control: ***, P < 0.001. Post-hoc Student's *t* test comparison between groups: ###, P < 0.001; ##, P < 0.01. Numbers above bars = *n*. Error bars show SEM.

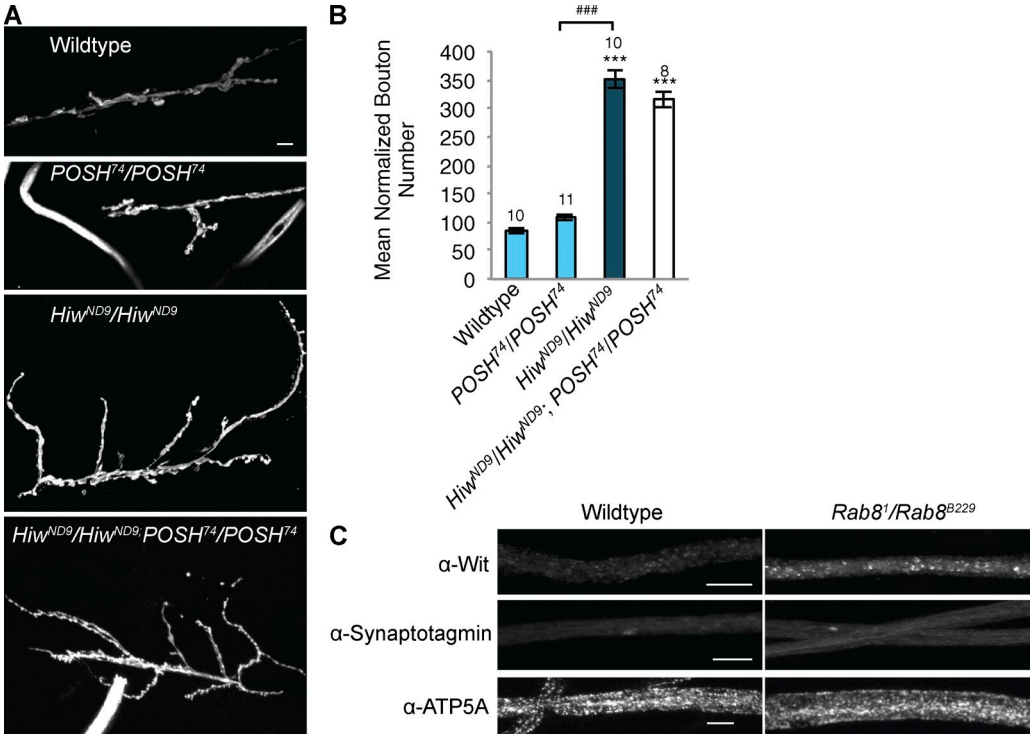

Figure S4. **POSH is not required for *Highwire*-induced synaptic overgrowth.** No general trafficking defect is observed in *Rab8* mutants. (A and B) Homozygous $POSH^{74}$-null alleles do not alleviate synaptic overgrowth in a Hiw^{ND9} mutant background. ANOVA: F(d.f. 3) = 181.469; P < 0.001 with post-hoc Dunnett's comparison to wild-type control: ***, P < 0.001. Post-hoc Student's *t* test comparison between groups: ###, P < 0.001. Numbers above bars = *n*. Error bars show SEM. (C) *Rab8* mutants do not show a general trafficking defect. Trafficking of synaptotagmin, Wit, and mitochondria appear normal in *Rab8* mutants, though levels of Wit appear elevated. Bars, 10 µm.

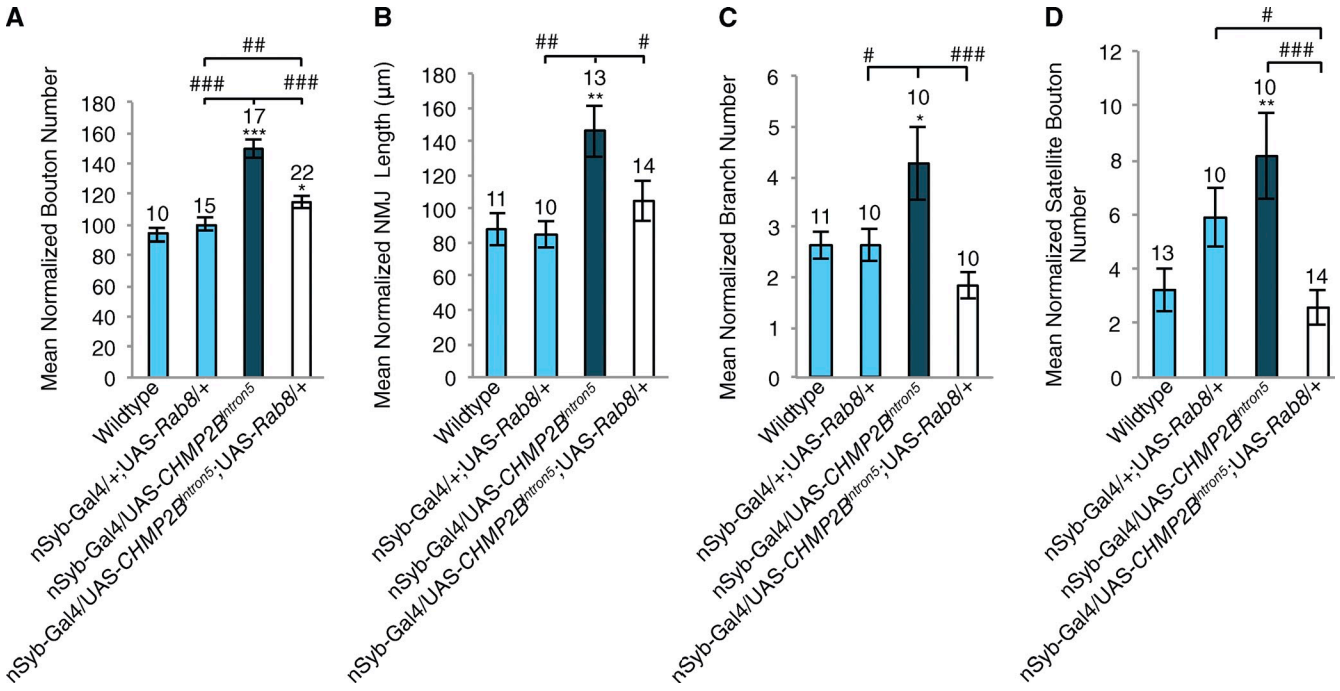

Figure S5. **Neuronal expression of Rab8 rescues neuronal perturbations associated with expression of the *CHMP2B*^{Intron5} transgene.** (A) Panneuronal expression of UAS-*CHMP2B*^{Intron5} induced a significant increase in synaptic bouton number at muscle 6/7, hemisegment A3, of third instar larvae. Increased bouton number could be rescued by coexpression of UAS-*Rab8*. ANOVA: F(d.f. 3) = 25.2705; P < 0.001 with post-hoc Dunnett's comparison to wild-type control: ***, P < 0.001; *, P < 0.05. Post-hoc Student's *t* test comparison between groups: ###, P < 0.001; ##, P < 0.01. (B) Panneuronal expression of UAS-*CHMP2B*^{Intron5} induced a significant increase in NMJ length at muscle 4, hemisegment A3, of third instar larvae. Increased NMJ length could be rescued by coexpression of UAS-*Rab8*. ANOVA: F(d.f. 3) = 5.4519; P < 0.01 with post-hoc Dunnett's comparison to wild-type control: **, P < 0.01. Post-hoc student *t* test comparison between groups: ##, P < 0.01; #, P < 0.05. (C) Panneuronal expression of UAS-*CHMP2B*^{Intron5} induced a significant increase in NMJ branch number at muscle 4, hemisegment A3, of third instar larvae. Increased branch number could be rescued by coexpression of UAS-*Rab8*. ANOVA: F(d.f. 3) = 5.4544; P < 0.01 with post-hoc Dunnett's comparison to wild-type control: *, P < 0.05. Post-hoc Student's *t* test comparison between groups: ###, P < 0.001; #, P < 0.05. (D) Panneuronal expression of UAS-*CHMP2B*^{Intron5} induced a significant increase in satellite bouton number at muscle 4, hemisegment A3, of third instar larvae. Satellite bouton number could be rescued by coexpression of UAS-*Rab8*. ANOVA: F(d.f. 3) = 6.5642; P < 0.001 with post-hoc Dunnett's comparison to wild-type control: **, P < 0.01. Post-hoc Student's *t* test comparison between groups: ###, P < 0.001; #, P < 0.05. Numbers above bars = *n*. Error bars show SEM.